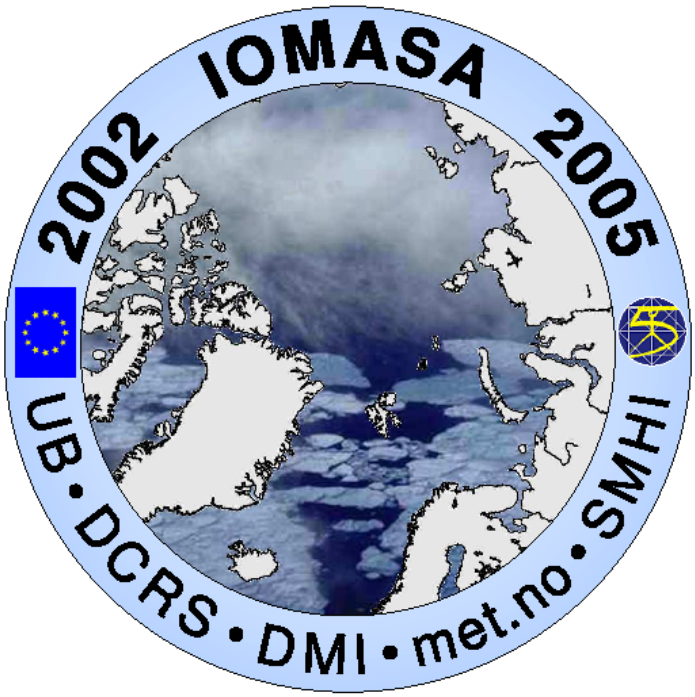

Report for IOMASA deliverable 3.2.2

ESTIMATING ICE, OCEAN AND ATMOSPHERIC PARAMETERS FROM POLAR REGIONS FROM AMSR-E MICROWAVE RADIOMETER MEASUREMENTS

DORTHE HOFMANN-BANG

LEIF TOUDAL PEDERSEN

DANISH CENTER FOR REMOTE SENSING

ØRSTED*DTU

TECHNICAL UNIVERSITY OF DENMARK

TABLE OF CONTENTS

1 Abstract

This report describes how the geophysical parameters wind speed, water vapor, liquid water, sea surface temperature, sea ice temperature, sea ice concentration and multi year ice fraction can be retrieved from AMSR data. The report describes a forward model for open water and the atmosphere, and an inverse algorithm and how the contribution from sea ice can be included in these. The model and the algorithm are verified by comparison with SSM/I retrievals, with ocean and atmosphere retrievals by Remote Sensing Systems, with SST data from the Ocean and Sea Ice SAF and with sea ice concentrations and MY-fractions of the NASA Team and Comiso Bootstrap sea ice algorithms. Finally some examples of retrieval of the geophysical parameter are shown, and the results obtained for each of the geophysical parameters are discussed.

2 Introduction

With the AMSR satellite microwave radiometer on-board the EOS-AQUA satellite it is possible to obtain long time series of brightness temperatures over the ocean. From the brightness temperatures geophysical parameters important for studying the global hydrologic cycle and the Earth's radiation budget, can be retrieved. The parameters, which can be retrieved, are two of the three phases of atmospheric water – vapor and liquid. Furthermore, surface parameters such as the near-surface wind speed, the sea surface temperature, the sea ice concentration and the sea ice type can be retrieved.
This document first describes a forward model, which relates the geophysical parameters to brightness temperatures measured by the AMSR. The forward model for open water/atmosphere is described by Wentz 2002. In the present document it is explained how the model can be expanded so it also includes ice covered surfaces. Next, the document describes a statistical method on how the geophysical parameters can be retrieved from the measured brightness temperatures. Then, the document includes a section on how the model has been verified and a section with some examples of the use of the retrieval algorithm. Finally the document ends with a summary of the results obtained by the examples and a discussion of the results.

3 Theory

3.1 Forward Model

Radiative transfer theory provides the relationship between the observed brightness temperatures T_B (K) and some geophysical parameters. A model describing this relationship is known as a forward model, and here a forward model described by Wentz 2002 has been used. The model describes the connection between 4 geophysical parameters (wind, water vapor, liquid water and sea surface temperature) and the brightness temperatures measured by the AMSR. The model described by Wentz 2002 is only valid for water surfaces, so the model has to be expanded to take ice covered surfaces in to account.

3.1.1 Inclusion of ice in the Forward Model

In the model by Wentz 2002 the upwelling brightness temperature at the top of the atmosphere - the brightness temperature measured by the AMSR satellite - is written in equation (10) as:

$$T_{B\uparrow} = T_{BU} + t\left[ET_S + T_{B\Omega}\right]$$

where T_{BU} is the contribution of the upwelling atmospheric emission, t is the total transmittance from the surface to the top of the atmosphere, E is the Earth surface emissivity and $T_{B\Omega}$ is the surface scattering integral.
A change in the surface content from open water to ice only have an influence on the following parts of the model: ET_s (the brightness temperature close to the sea surface) and $T_{B\Omega}$.
In order to be able to include ice in the model for the brightness temperature close to the sea surface, one has to consider the difference between the emissivity of an open water sea surface and an ice covered sea surface.
The brightness temperature, $T_{B,ice}$, at the ice surface can be written as:

$$T_{B,ice} = T_{p,ice} \cdot E_{ice}$$

where $T_{p,ice}$ is the physical temperature of the ice surface and the E_{ice} is the emissivity of the ice surface.
The emissivity of an ice covered surface is dependant on the type of ice cover, the polarization and the frequency. The sea ice emissivities used to calculate the brightness temperatures of the different channels of the AMSR are given in the Table 3-1.

Freq		6GHz	10GHz	18GHz	23GHz	37GHz
FY	Vertical	0.9204	0.9127	0.9373	0.9409	0.9347
	Horizontal	0.7502	0.7738	0.8314	0.8490	0.8600
MY	Vertical	0.9692	0.9284	0.8843	0.8554	0.7813
	Horizontal	0.8651	0.8356	0.7917	0.7792	0.7248

Table 3-1 The table shows the emissivities for the First Year (FY) and Multi Year (MY) ice used in the forward model.

Now, the brightness temperature close to a surface mixed of open water, FY and MY ice can be written as:

$$T_{B,S} = ET_S = C_{ow}T_{B,ow} + C_{FY}T_{B,FY} + C_{MY}T_{B,MY}$$

where C_{FY}, C_{MY} and C_{ow} are the concentrations of open water and sea ice, and $T_{B,ow}$, $T_{B,FY}$ and $T_{B,MY}$ are the brightness temperatures of the three different surface types.

The surface scattering integral is given in Wentz 2002, equation (61) as:

$$T_{B\Omega} = [(1+\Omega)(1-t)(T_D - T_C) + T_C]R$$

In this equation it is only the sea-surface reflectivity R, which is influenced by the ice. An effective reflectivity for a mixed surface can be written as:

$$R_{eff,mix} = 1 - E_{eff,mix} = 1 - (C_{ow}E_{ow} + C_{FY}E_{FY} + C_{MY}E_{MY})$$

where C_{ow}, C_{FY} and C_{MY} are the concentrations of the three surface types and E_{ow}, E_{FY} and E_{MY} are the emissivity of the surface types.

The last thing one has to take in to consideration, when including ice in the model, is that the forward model described by Wentz 2002 has a surface temperature included. This temperature has to take the temperature of the ice into account and therefore the surface temperature used in the ice model, has to be calculated by:

$$T_{S,mix} = C_{ice} \cdot T_{P,ice} + C_{ow} \cdot T_{P,ow}$$

where C_{ice} and C_{ow} is the concentration of open water and sea ice, and $T_{P,ice}$ and $T_{P,ow}$ are the surface temperatures. This mixed surface temperature only has to be used in the part of the model concerning the atmosphere, not in the parts concerning the dielectric constant of sea-water and the wind-roughened sea surface.

3.2 Inverse Model

The inverse model is used to retrieve the geophysical parameters from the brightness temperatures measured by the AMSR.
The inverse model used here is described by Rodgers 1976, and is based on an approximated linear function, which can be written in a discrete version as:

$$\mathbf{T_A} = \mathbf{Mp} + \mathbf{e}$$

where $\mathbf{T_A}$ is the brightness temperatures, $\mathbf{p}$ is the geophysical parameters, $\mathbf{e}$ is the normal distributed error with the covariance matrix $\mathbf{S_e}$ and $\mathbf{M}$ is the mixing matrix and contains the partial derivatives, and can be written as:

$$M_{ij} = \frac{\partial T_{Ai}}{\partial p_j}$$

A least square solution can be found for the linear function. The solution can be improved be including á priori information, and an expression for the estimated parameters, $\hat{p}$, can be written as:

$$\hat{\mathbf{p}} = \hat{\mathbf{S}}\left(\mathbf{S_p^{-1}}\mathbf{p_0} + \mathbf{M^t}\mathbf{S_e^{-1}}\mathbf{T_A}\right)$$
$$\hat{\mathbf{S}} = \left(\mathbf{S_p^{-1}} + \mathbf{M^t}\mathbf{S_e^{-1}}\mathbf{M}\right)^{-1}$$

where $\hat{\mathbf{S}}$ is the covariance matrix of the estimated parameters, $\mathbf{S_p}$ is the covariance matrix of the á priori information and $\mathbf{p_0}$ is the mean values of the á priori information.
The equations are solved by using the method of Newtonian iteration. Newtonian iteration is described by Rodgers 1976 and is simply a matter of expanding the model as a Taylor series about a guessed value of the solution p_n. This can be written as:

$$\mathbf{p}_{n+1} = \mathbf{p}_n + \left(\mathbf{S}_p^{-1} + \mathbf{M}_n^T\mathbf{S}_e^{-1}\mathbf{M}_n\right)^{-1}\left(\mathbf{M}_n^T\mathbf{S}_e^{-1}\left(\mathbf{T}_A - \mathbf{T}_{A,n}\right) + \mathbf{S}_p^{-1}\left(\mathbf{p}_0 - \mathbf{p}_n\right)\right)$$

$\hat{\mathbf{p}}$ has been replace in the equation by p_{n+1} because this is an iterative equation , and $\mathbf{p_n} \to \hat{\mathbf{p}}$ *as* $n \to \infty$.

In order to be able to estimate the geophysical parameters the covariance matrix, $\mathbf{S_e}$ of the AMSR data and the á priori information has to be known. The covariance matrix of the measurements is showed in Table 3-2 (Reference: NASDA 2003).

	6V	6H	10V	10H	18V	18H	23V	23H	37V	37H
6V	0.09	0	0	0	0	0	0	0	0	0
6H	0	0.1089	0	0	0	0	0	0	0	0
10V	0	0	0.2209	0	0	0	0	0	0	0
10H	0	0	0	0.2916	0	0	0	0	0	0
18V	0	0	0	0	0.2304	0	0	0	0	0
18H	0	0	0	0	0	0.2116	0	0	0	0
23V	0	0	0	0	0	0	0.2025	0	0	0
23H	0	0	0	0	0	0	0	0.1936	0	0
37V	0	0	0	0	0	0	0	0	0.2025	0
37H	0	0	0	0	0	0	0	0	0	0.16

Table 3-2 The table shows the covariance matrix of the AMSR measurements. Reference: (NASDA 2003)

The á priori information used in the calculations is showed in Table 3-3 and Table 3-4. The covariance matrix has except for the sea ice temperature been calculated from a high resolution limited area model (HIRLAM). HIRLAM is a mesoscale atmospheric model operated at the Danish Meteorological Institute for analysis and forecast in the weather service. The data set covers the period from the 28th of March 2003 at 07.00 (UTC) to the 2nd of April 2003 at 05.00 (UTC). We have not been able to obtain any information about the sea ice temperature, and therefore the standard deviation (the diagonal elements in the covariance matrix) for the sea ice temperature has been set to the same value as the open water temperature. Furthermore because there is not á priori information about the sea ice temperature the off diagonal elements for the sea ice temperature have been set to 0.
Concerning the mean values, the first four values in the table has also been calculated from the HIRLAM data set. The last three values have been calculated by some simple algorithms, which are explained in the references.

	W	V	L	Tow	Tis	Cis	FMY
W	12.3024	3.2072	0.1398	6.0322	0	-0.6525	-0.9347
V	3.2072	11.0481	0.2495	11.9348	0	-0.3085	-0.5362
L	0.1398	0.2495	0.0204	0.2041	0	-0.0063	-0.0152
Tow	6.0322	11.9348	0.2041	23.9468	0	-0.7254	-1.0207
Tis	0	0	0	0	23.9468	0	0
Cis	-0.6525	-0.3085	-0.0063	-0.7254	0	0.0114	0.1203
FMY	-0.9347	-0.5362	-0.0152	-1.0207	0	0.1203	0.0332

Table 3-3 The table shows the covariance matrix for the á priori information.

W	V	L	Tow	Tis	Cis	FMY
4.9533	3.6164	0.0808	274.5	calc	calc	calc

Table 3-4 The table shows the mean values for the á priori information. The values marked with calc, is calculated using some simpler algorithms (Reference: Comiso et. Al. 1997 and Cavalieri et. Al. 2000)

As described earlier the process of estimating the geophysical parameters is an iterative process. After some investigations it has been decided always to make 5 iterations for each measurement. After the 5th iteration a test value is calculated in order to have a measure of how good the estimation is. The test value is calculated as the square root of the sum of the error for each of the AMSR channels. The error is calculated as the difference between the measured brightness temperature and the brightness temperature calculated by the forward model from the estimated geophysical parameters.

4 Verification

4.1 Comparison of SSM/I vs. AMSR - synthetic data

In order to verify that the model without ice works, a test has been carried out with synthetic data. 4 synthetic data sets, which contain brightness temperatures, have been calculated by the forward model. For each data set one of the geophysical parameters has been varied over an interval, while the rest have been kept on a default value. The default values are shown in Table 4-1.

Parameter	**Default value**
Wind speed [m/s]	8
Water vapor [mm]	10
Liquid water [mm]	0.05
Sea surface temperature [K]	275

Table 4-1 Default parameters used for simulation.

The data sets have been used as input to the inverse function, and finally the difference between the input parameter to the forward function and the estimated parameter has been calculated. The results of the simulation - the difference between the input and output parameter - can be seen for each of the 4 data sets in Figure 4-1, Figure 4-2, Figure 4-3 and Figure 4-4. For reference the simulations have been carried out for synthetic data sets for AMSR and SSM/I (The SSM/I forward model is described by Wentz 1997). Furthermore the standard deviations of the estimates are also showed in the figures.

When looking at the graphs it can be seen, that the estimated parameters are quite accurate and, that they have low standard deviations. When comparing the results from the AMSR model with the results from the SSM/I model it can be seen, that in general the AMSR gives the best result. But, when looking at the sea surface temperatures, the SSM/I model obtains better results than the AMSR model. The explanation for this is probably that the SSM/I do not have the low frequency channels (6 and 10GHz) included, and it is these channels which contains most information about the temperature variations. Therefore the retrieval of the sea surface temperature form the SSM/I data are mostly based on the á priori information. This is discussed further in section 4.3 “Test of exclusion of the 6GHz and 10GHz channels”. Concerning the standard deviation of the liquid water content the SSM/I model also obtains the smallest values.

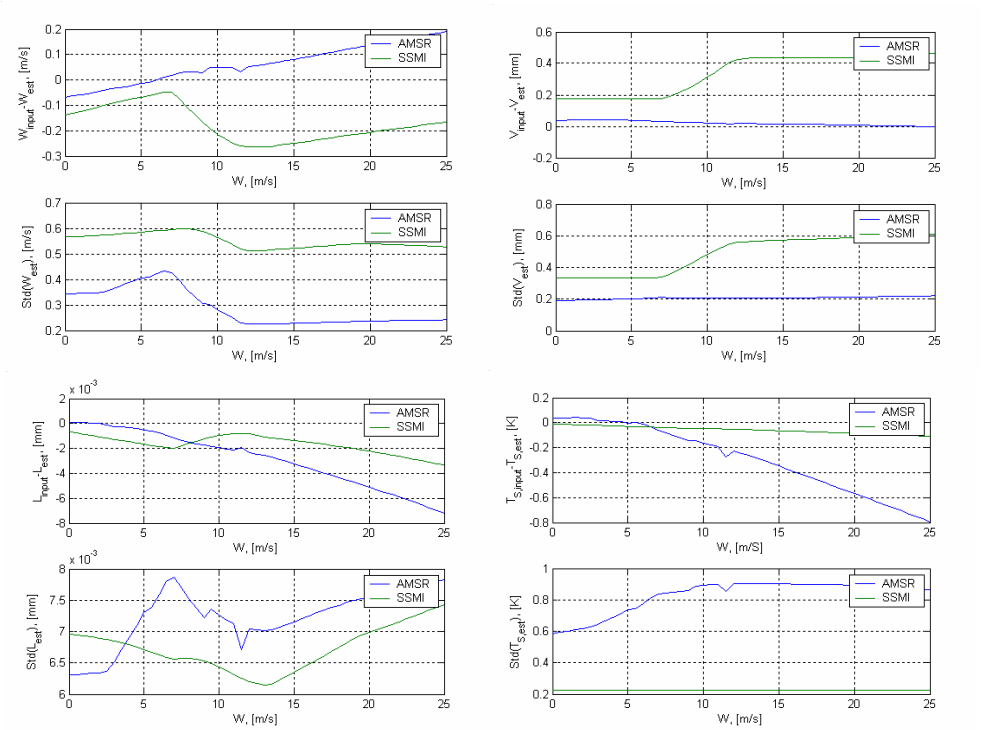

Figure 4-1 Comparison between the geophysical parameters estimated from SSM/I and AMSR data as a function of the wind speed. The figure contains 2 graphs for each parameter. The first graph shows the difference between the input parameter in the forward model and the output parameter from the inverse model. The second graph shows the standard deviation of the estimated parameters.

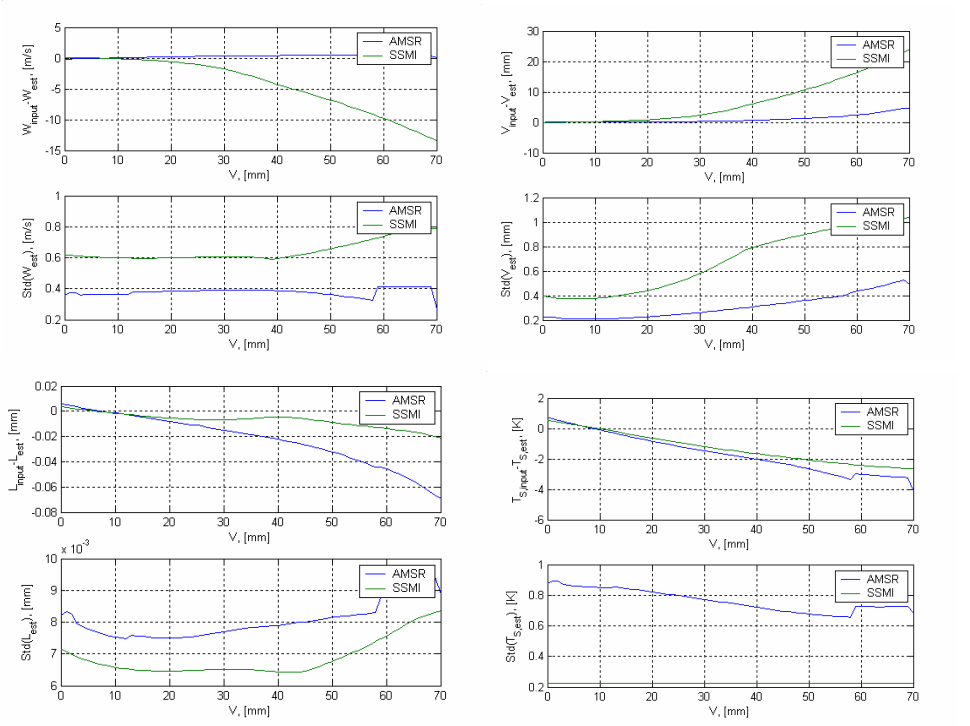

Figure 4-2 Comparison of the geophysical parameters estimated from SSM/I and AMSR data as a function of the water vapor. The figure contains 2 graphs for each parameter. The first graph shows the difference between the input parameter in the forward model and the output parameter from the inverse model. The second graph shows the standard deviation of the estimated parameters.

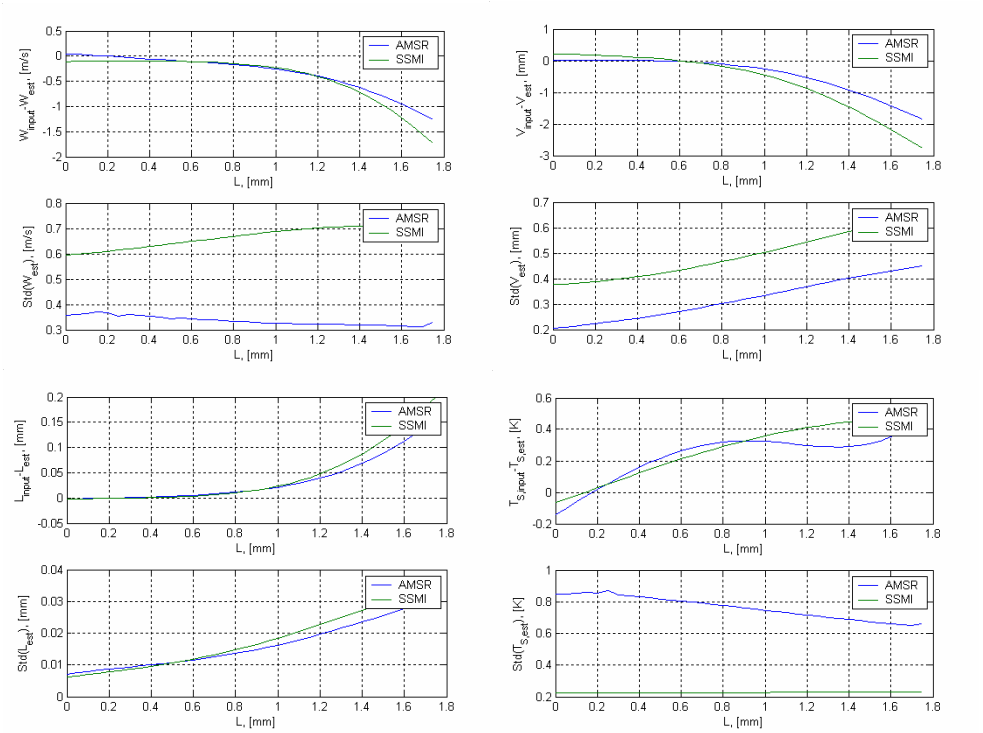

Figure 4-3 Comparison of the 4 geophysical parameters estimated from SSM/I and AMSR data as a function of the liquid water. The figure contains 2 graphs for each parameter. The first graph shows the difference between the input parameter in the forward model and the output parameter from the inverse model. The second graph shows the standard deviation of the estimated parameters.

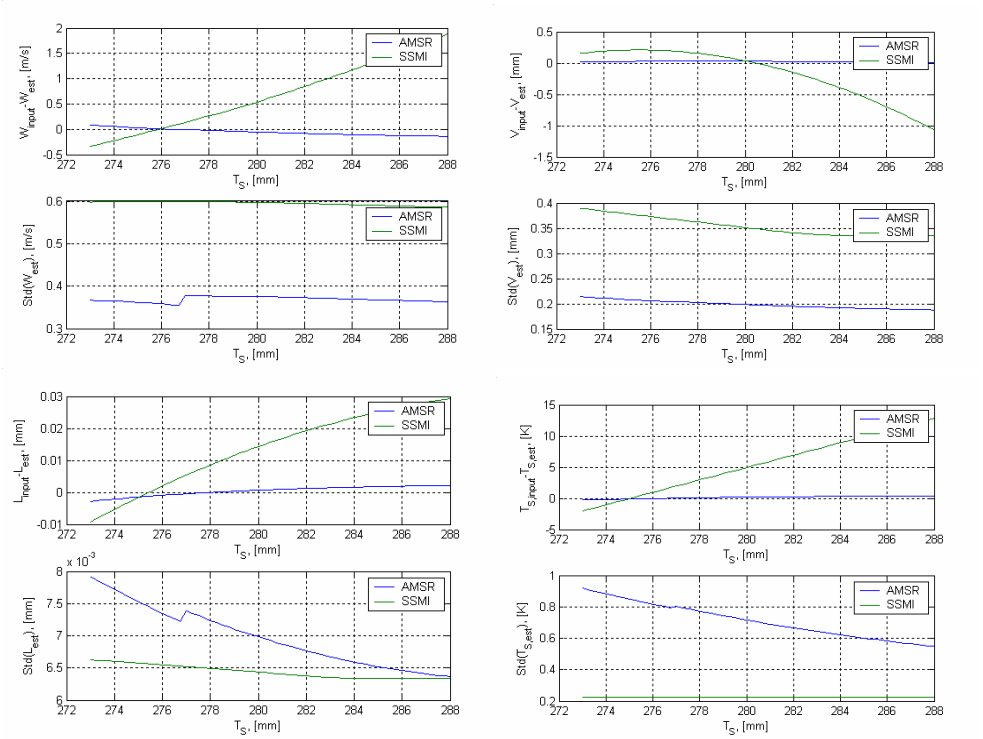

Figure 4-4 Comparison of the 4 geophysical parameters estimated from SSM/I and AMSR data as a function of the sea surface temperature. The figure contains 2 graphs for each parameter. The first graph shows the difference between the input parameter in the forward model and the output parameter from the inverse model. The second graph shows the standard deviation of the estimated parameters.

4.2 Comparison between the model with and without ice

In order to compare the original model and the model, which has ice included; the two algorithms have been tested on a line of data from a satellite passage over the North Atlantic the 18th of November 2003. The data set contains scan element no. 150 and covers both open water and sea ice. The first 100 samples are samples from an ice-covered surface and a little bit of Svalbard. The samples 100 to 250 are measured over open water. The next 25 samples are land (Iceland), and finally the rest of the samples are again measured over open water. The line of data is shown in Figure 4-5. In this figure the line of data is shown on top of an ice concentration image and on top of an image of the amount of liquid water, so it can be seen what the data line contains.

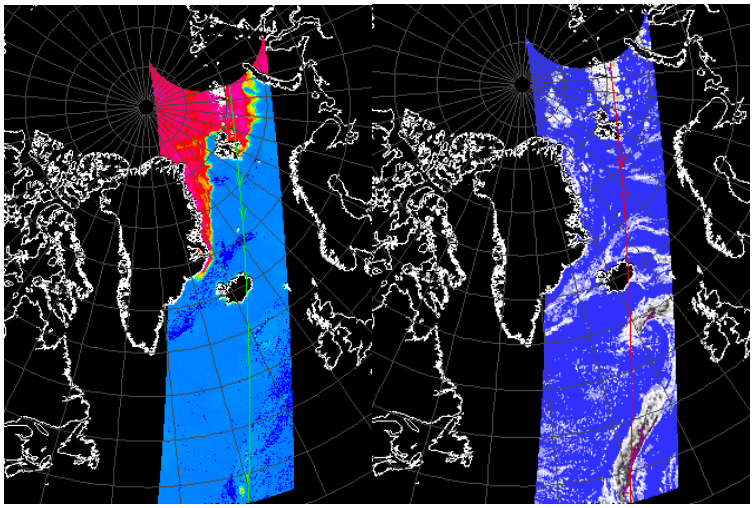

Figure 4-5 To the left is a map of the sea ice concentration, and to the right is a map of the amount of liquid water. On the two maps is the placement of the line of data illustrated as a green or a read line.

The estimated geophysical parameters from the data set are shown on Figure 4-6 to Figure 4-11. For each parameter the estimated value and the standard deviation is shown.

When looking at the figures it can be seen, that the wind can not be estimated over the sea ice surface. This is logical because the wind speed is retrieved mainly from the microwave signature of the wind induced sea surface roughness, which is missing over the sea ice. When looking at the wind speed estimated over open water it can be seen, that by including ice in the forward model the standard deviation increases, e.g. the retrieval becomes more uncertain.

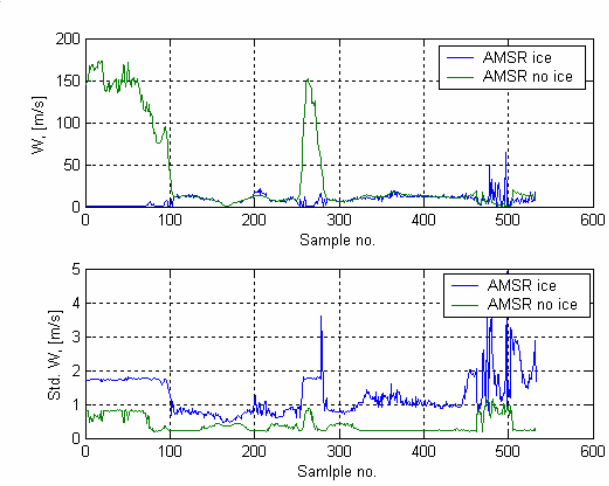

Figure 4-6 The first graph shows the estimated wind speed for the two models, and the second graph shows the standard deviation of the estimated wind speeds.

Looking at the estimated water vapor and liquid water in Figure 4-7 and Figure 4-8, it can be seen, that over open water it does not matter whether ice is included in the model or not. On the other hand, when ice is included in the model, it is possible to estimate the amount of water vapor or liquid water over the ice surface, but with a higher standard deviation than over the open water surface. Typical Standard deviations of V are 0.3 mm over ocean and 1 mm over ice.

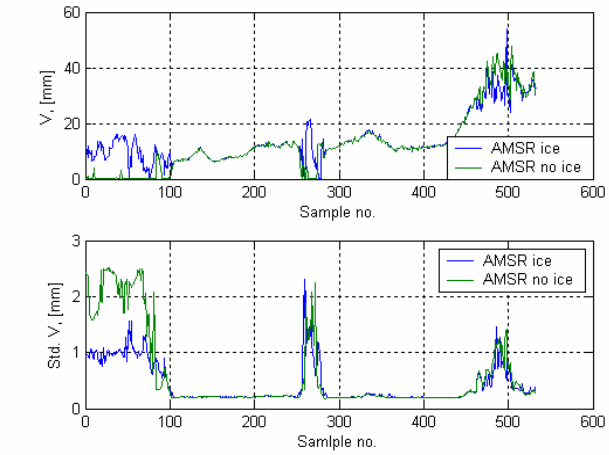

Figure 4-7 The first graph shows the estimated water vapor for the two models, and the second graph shows the standard deviation of the estimated water vapor.

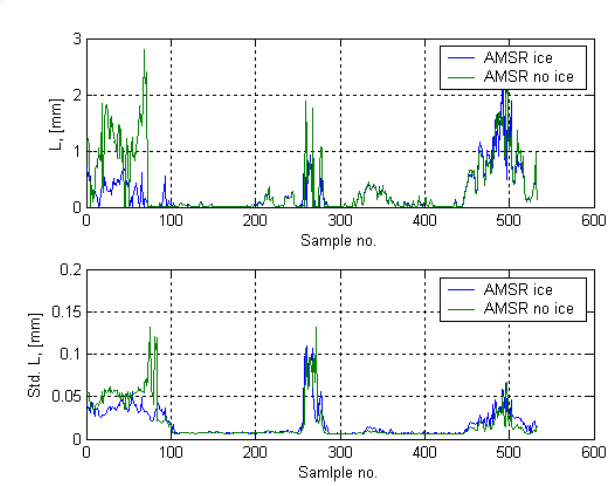

Figure 4-8 The first graph shows the estimated liquid water for the two models, and the second graph shows the standard deviation of the estimated liquid water.

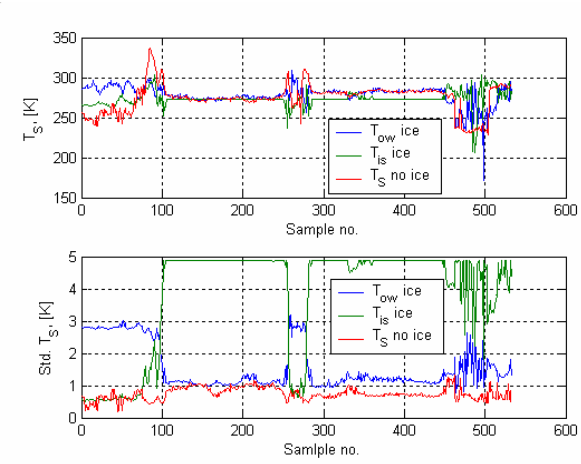

Figure 4-9 The first graph shows the estimated temperatures for the two models, and the second graph shows the standard deviation of the estimated temperatures. The graphs show 3 temperatures because the model with ice contains two temperatures – the ice temperature and the open water temperature – and the model without ice only contains one temperature namely the sea surface temperature (which is the open water temperature).

When considering the surface temperatures in Figure 4-9, it can be seen, that the ice temperature estimated by the original model is not correct. On the other hand when looking at the model with ice, it can be seen, that the temperature of the ice and the temperature of the open water are being estimated correctly according to the surface type. Comparing with the ice concentration it can be seen, that the standard deviation of the two temperatures indicate, which of the temperatures is the correct one representing the current surface type.

Figure 4-10 and Figure 4-11 shows the results of the estimation of the ice parameters, estimated only by the algorithm where ice is included. From the figures it can be seen, that the ice concentration is estimated quite well with a standard deviation of about 1-2%. It is only in the end of the data line (around sample no. 475), that some noise appears; this is due to the large amount of liquid water in the atmosphere at this location (see Figure 4-5). When considering the multi year ice fraction, it can be seen, that over the ice surface the fraction is being estimated quite well. On the other hand over the open water the multi year ice fraction takes strange values, but again this is indicated by

an increased standard deviation, and is considered less important since the ice concentration is very low.

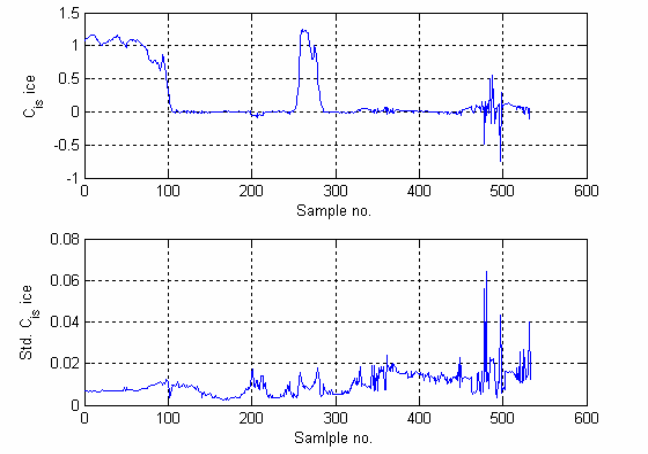

Figure 4-10 The first graph shows the estimated ice concentration for the ice model, and the second graph shows the standard deviation of the estimated ice concentration.

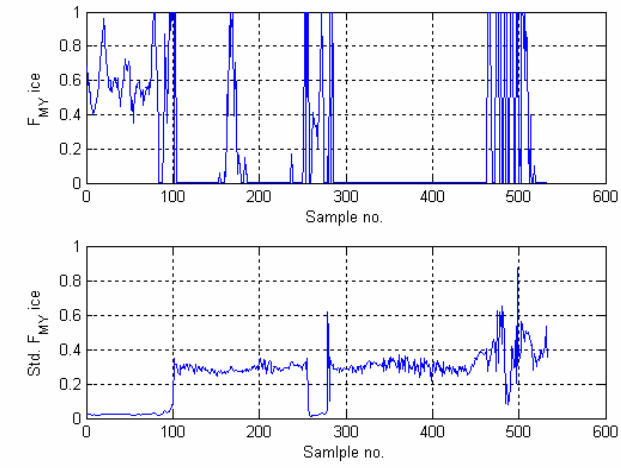

Figure 4-11 The first graph shows the estimated multi year ice fraction for the ice model, and the second graph shows the standard deviation of the estimated multi year ice fraction.

In Figure 4-12 the test value of the estimation is shown. From the test value it is clearly indicated, that the inclusion of ice in the model makes it easier for the model to make the brightness temperatures fit to the geophysical parameters over the ice surface. Furthermore it does not look like the inclusion of ice has influence on the estimation of the geophysical parameters over open water except for the area, which has a high content of liquid water (around sample 475). The increased test value over the cloud of liquid water can not be explained at the moment. We have tried to solve the problem by increasing the amount of iterations, but it did not solve the problem. At the moment we come around the problem by removing the retrieved geophysical parameters, which has a high test value. But of cause the problem should be a topic for further investigations in the future.

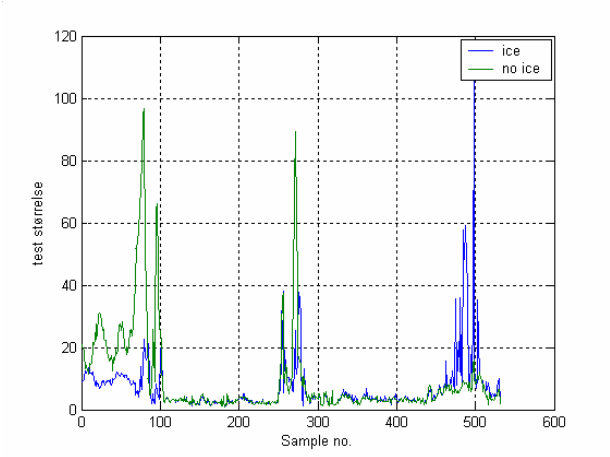

Figure 4-12 Test value.

4.3 Test of exclusion of the 6GHz and 10GHz channels

In order to figure out how much the inclusion of the low frequency channels 6.9GHz and 10.7GHz means for the estimation of the geophysical parameters, a test has been carried out for the same data line as used in the previous section. The test has been carried out for the ice model, and first the exclusion of the 6GHz cannel has been tested, and then the exclusion of both the 6GHz and the 10GHz has been tested.

The way the channels have been excluded from the estimation is by setting the appropriate element in the covariance matrix for the measurements, $\mathbf{S_e}$ to a high value (it has been set to 100000). The result of the test is shown in Figure 4-13 to Figure 4-20. On each of the figures the graphs from the two tests are shown together with the graph for the estimation where all the AMSR channels are included.

For the estimation of the wind speed the exclusion of the low frequency channels only has an influence if there is a lot of water in the atmosphere.

For the estimation of water vapor and liquid water the exclusion of the low frequency channels has a large influence on both the estimation of the parameters and the standard deviation of the estimate over the ice covered surface, but not over the water surface. The error of the estimated parameter and the standard deviation increases when the 6GHz channel is excluded and even more, when both the 6GHz and the 10GHz channels are excluded.

When looking at the sea surface temperatures it has a large influence on the estimated value and on the standard deviation of the open water temperature to exclude the 6GHz channel, but it nearly does not make any differenced also to exclude the 10GHz channel. Concerning the ice surface temperature the standard deviation increases when the low frequency channels are being excluded, but not as much as for the open water temperature. Furthermore the 10GHz channel has an influence on the estimated value.

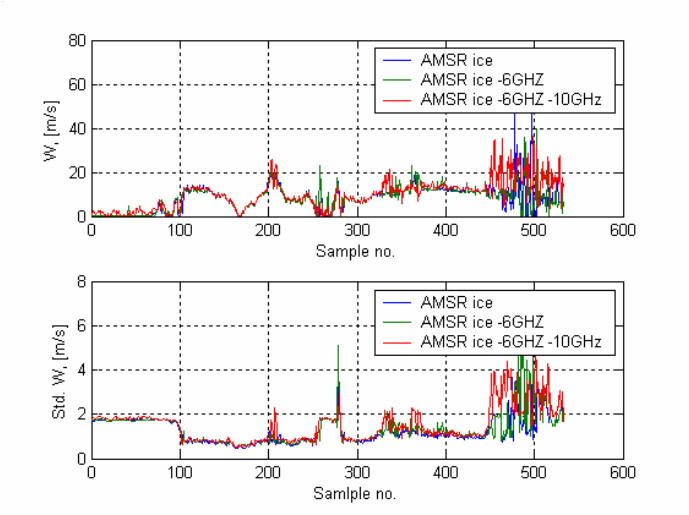

Figure 4-13 Estimate and standard deviation of the wind speed.

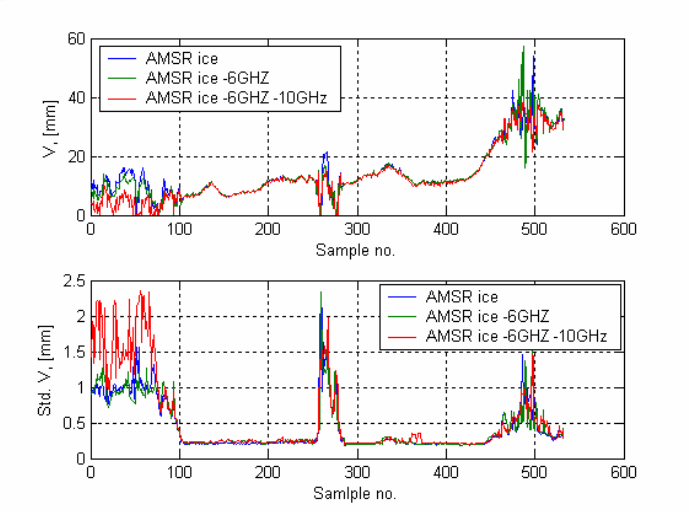

Figure 4-14 Estimate and standard deviation of the water vapor.

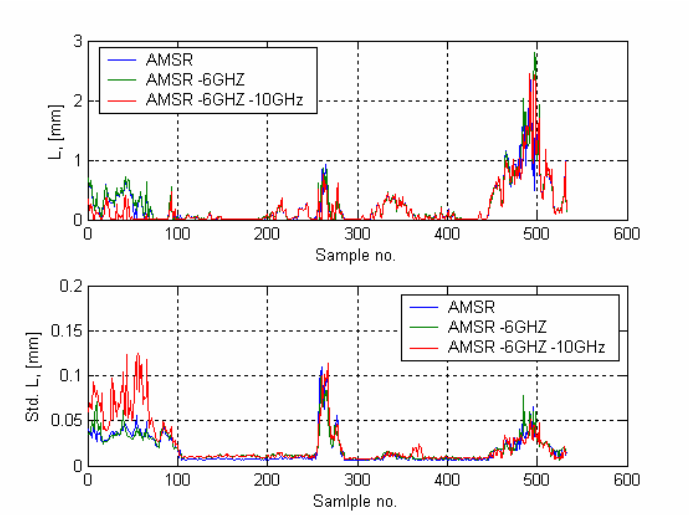

Figure 4-15 Estimate and standard deviation of the liquid water.

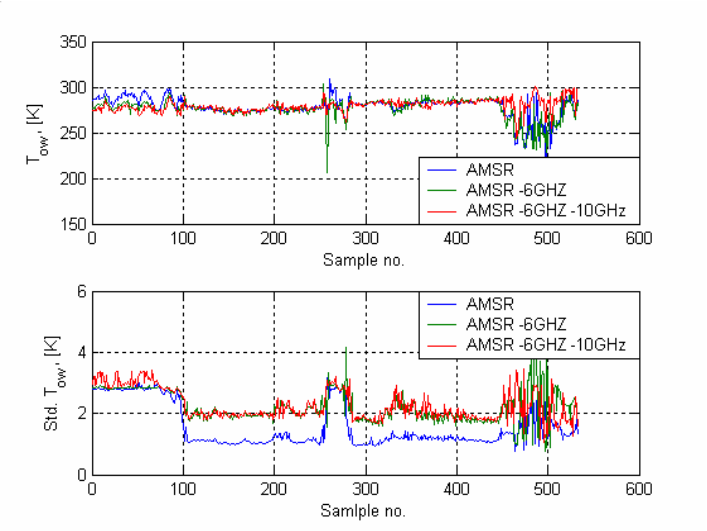

Figure 4-16 Estimate and standard deviation of the open water temperature.

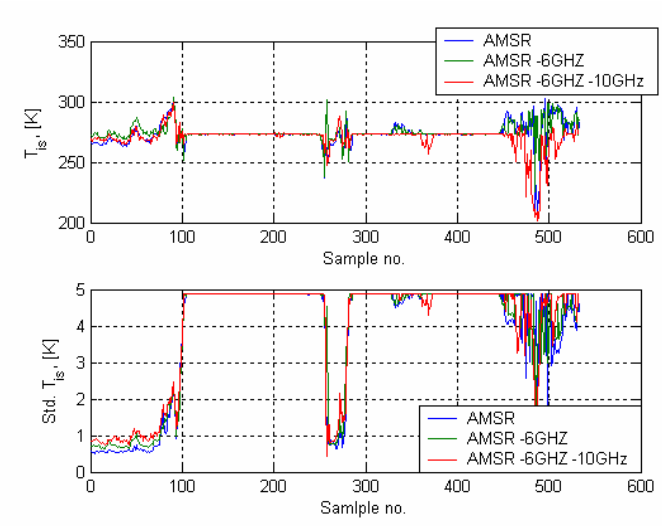

Figure 4-17 Estimate and standard deviation of the sea ice temperature.

For the ice concentration it looks like the removal of the low frequency channels only has an influence on the standard deviation of the result over water, where there is a lot of water in the atmosphere. On the other hand for the multi year ice fraction the exclusion of the low frequency channels has an influence, but as shown on the graph, very little on the standard deviation of the estimate. This is particular true over the ice surface and when there is a lot of water in the atmosphere. When there is a lot of liquid water in the atmosphere the standard deviation of the multi year ice fraction increases.
When considering the test value, one can see that the exclusion of the low frequency channels makes the test value increase especially when there is a lot of liquid water in the atmosphere.
All in all it can be concluded that the low frequency channels have the greatest impact on the estimated parameters and the standard deviation where water and in particular liquid water is present in the atmosphere.

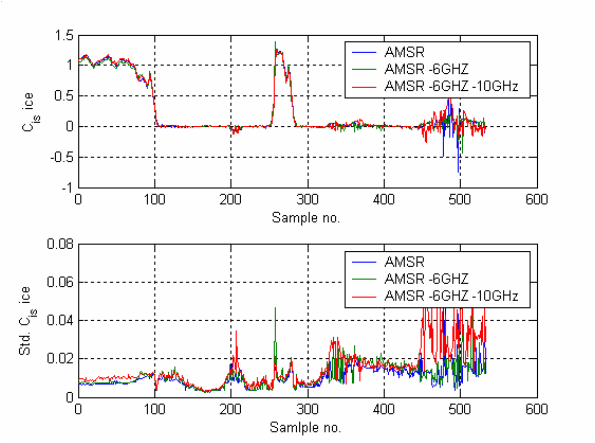

Figure 4-18 Estimate and standard deviation of the sea ice concentration.

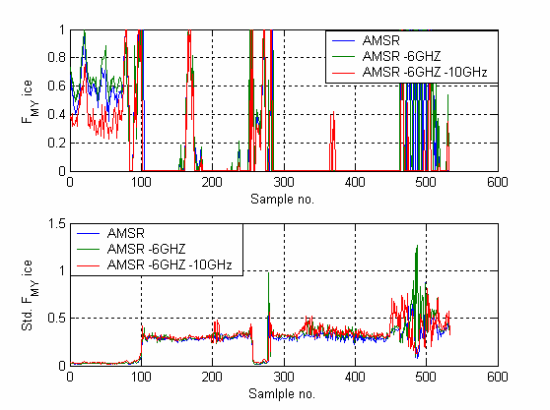

Figure 4-19 Estimate and standard deviation of the multi year ice fraction.

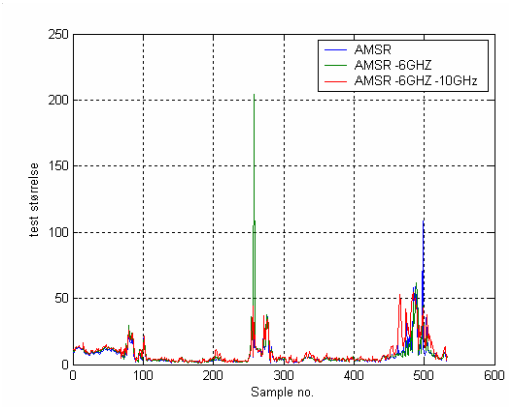

Figure 4-20 Test value.

4.4 Comparison with Wentz data

In order to verify the results obtained by the retrieval algorithm a comparison between our retrieved geophysical parameters and geophysical parameters from Remote Sensing System/Frank Wentz (downloaded from www.remss.com) has been carried out. The comparison for the 18th of November 2003 can be seen in Figure 4-21 to Figure 4-24 for the four geophysical parameters near surface wind speed, water vapor, liquid water and open water sea surface temperature. The model, which has ice included, has been used for our calculations. It is only the four showed parameters, which can be compared, because Wentz do not have sea ice included in his algorithm.

The four graphs show scatter plots of our geophysical parameters versus the geophysical parameters from Frank Wentz. When considering the four graphs the first thing to be noted is that the data of Frank Wentz is quantized and ours are not (this can be seen in some of the graphs as the vertical stripes in the data clouds).
When comparing the parameters, it can be seen, that there is clear linear relationship for three of the parameters (wind speed, water vapor and sea surface temperature). Concerning the liquid water parameter the linear relationship is not as clear as for the other parameters. For all four parameters the results are placed in a cloud around the x=y line (red line). For the wind speed the cloud of data is almost centered on the x=y line and therefore it looks like the two algorithms have about the same amount of data, which is over and under estimated. When looking at the results of the estimated water vapor, it looks like our algorithm almost always estimates a little more water vapor than the algorithm of Frank Wentz. For the graph of the liquid water it is difficult to see a clear linear relationship, but still all the estimated values are gathered in a cloud. When zooming in on the cloud it shows out, that most of the data is actually gathered around the x=y line, but maybe the data from our calculations have a little higher values than the results of Wentz. Finally, when considering the sea surface temperature, the cloud of data is also centered on the x=y line, but now it is the values of Wentz, which are a little higher than our results.
The mean values of the standard deviations of our calculations are showed in Table 4-2. It has not been possible to find the exact standard deviation for the calculations of the geophysical parameters by Wentz. Instead the table shows the expected standard deviation for the algorithm by Went (Wentz 2000). These standard deviations can contribute to some of the explanations of differences in the geophysical parameters retrieved from our algorithm and from Wentz' algorithm. Furthermore one has to remember, that it was showed 4.2 "Comparison between the model with and without ice", that the inclusion of ice in the algorithm has an influences on the standard deviation of the estimated parameters.

Parameter	**Our mean value of the standard deviation**	**Expected standard deviation for Wentz**
Wind speed [m/s]	1.22 m/s	1.0 m/s
Water vapor [mm]	0.38 mm	1.0 mm
Liquid water [mm]	0.013 mm	0.02 mm
Sea surface temperature [K]	1.48 K	0.5 K

Table 4-2 The table shows the mean of the standard deviation for 4 of the geophysical parameters estimated by our algorithm and the expected standard deviation for the estimation by Wentz (Wentz 2000).

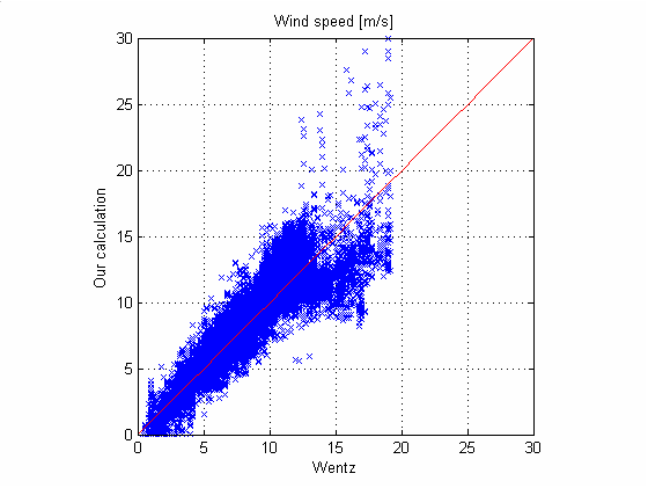

Figure 4-21 Comparison of the near surface wind speed calculated by Wentz and calculated by us. Data is from the 18th of November 2003.

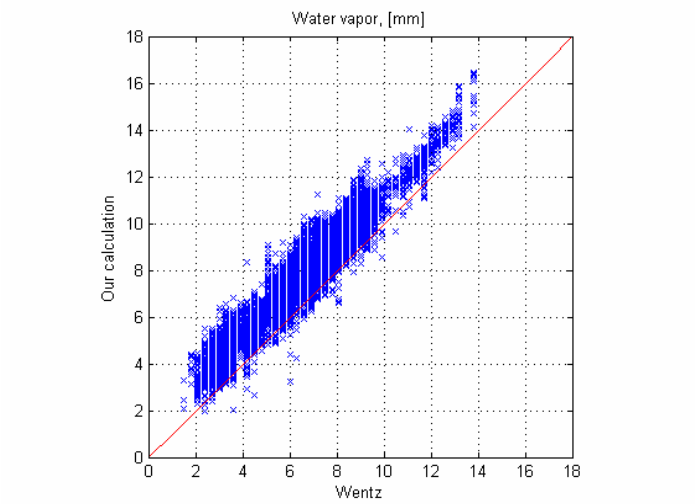

Figure 4-22 Comparison of the water vapor calculated by Wentz and calculated by us. Data is from the 18th of November 2003.

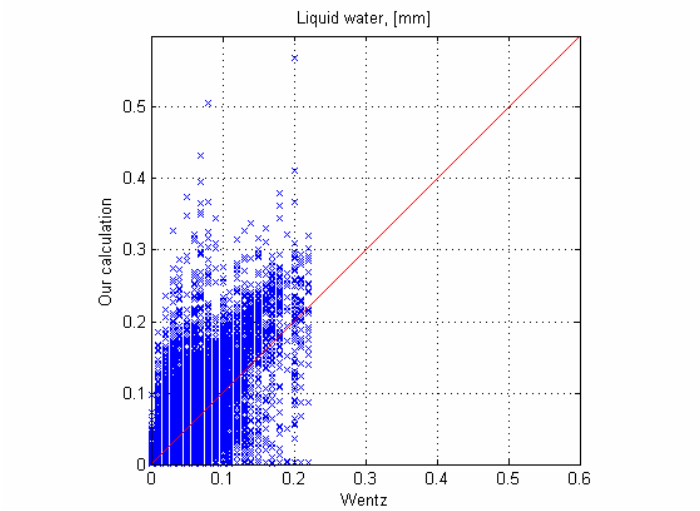

Figure 4-23 Comparison of the liquid water calculated by Wentz and calculated by us. Data is from the 18th of November 2003.

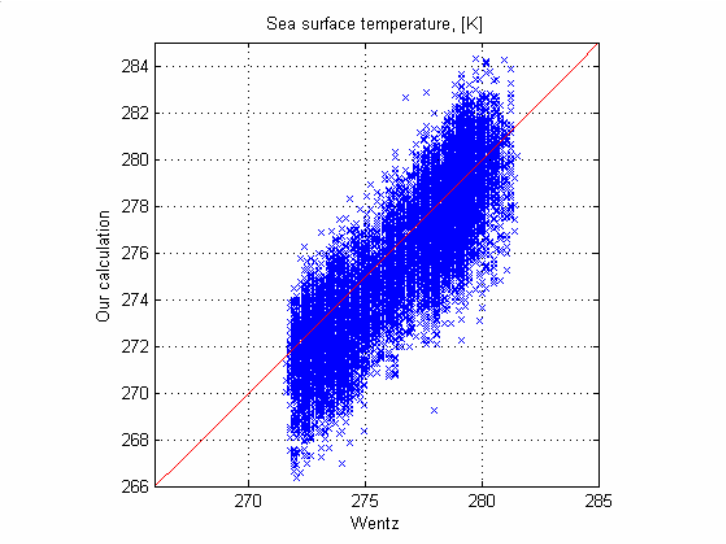

Figure 4-24 Comparison of the sea surface temperature calculated by Wentz and calculated by us. Data is from the 18th of November 2003.

4.5 SST comparison with O&SI SAF data

In order the verify the sea surface temperature (SST) a comparison with Ocean & Sea Ice Satellite Application (O&SI SAF) data has been carried out. The regional SST SAF data are derived form the NOAA/AVHRR data. The data has a resolution of 2 km and is available from the North Atlantic area every 6th hour (Météo-France, 2002).
The sea surface temperature has been compared for data form three different days. The result of the comparison can be seen in Figure 4-25 to Figure 4-27. From the three figures it can clearly be seen, that there is a linear relation ship between the two sea surface temperatures. The standard deviation of the SAF SST is 0.6-0.8K and the standard deviation for the SST retrieved by our algorithm is about 1.2K, and this might explain some of the variation in the three scatter plots.
In the scatter plots for the data in November there are two clouds of data, which has no linear relationship with the SAF SST. For these data our algorithm has estimated very low values, while the SAF data has values above 273^0K. It our sea surface temperatures, which are estimated wrongly and they occur due to an error in the AMSR radiometer as described in section 5 “Examples”.

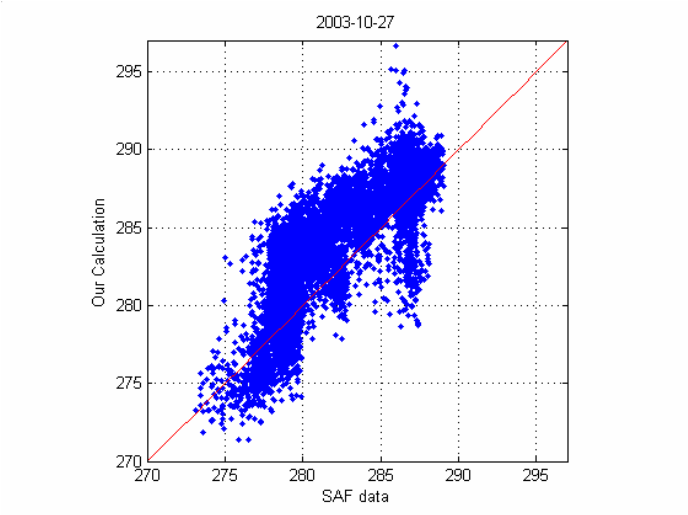

Figure 4-25 Scatter plot of the SAF surface temperature and our calculated surface temperature at the 27th of October 2003.

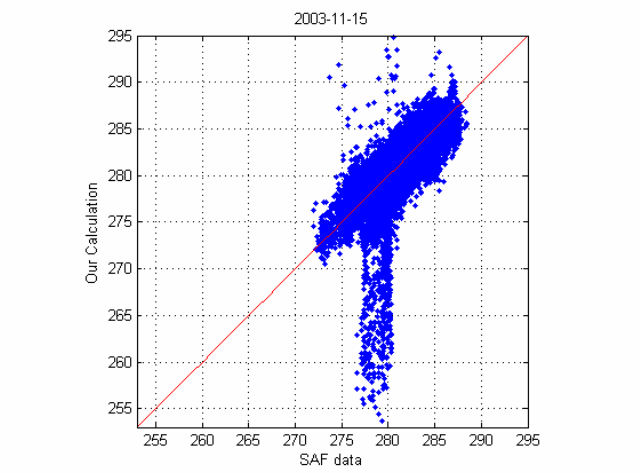

Figure 4-26 Scatter plot of the SAF surface temperature and our calculated surface temperature at the 15th of November 2003.

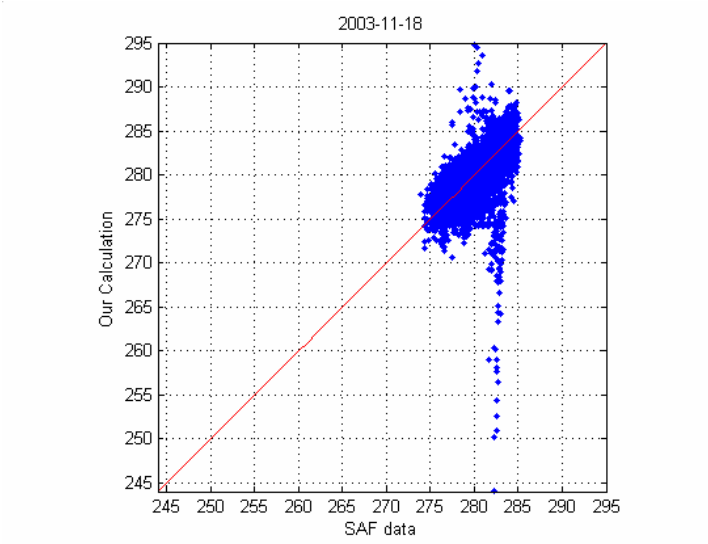

Figure 4-27 Scatter plot of the SAF surface temperature and our calculated surface temperature at the 18th of November 2003.

4.6 Sea ice comparison

In order to find out how well the algorithm estimates the sea ice concentration the results from our algorithm has been compared with results from the NASA Team Sea Ice Algorithm. The comparison has been carried out for two types of data set. The first type of data is one, which contains one line in the AMSR scan at a specific satellite passage. The second type of data is a time series of data from a specific location.

4.6.1 Comparison with line of data

A data set with a line of data from a satellite passage the 18th of November 2003 has been use as an example. The data set is the same as the one described in section 4.2 ”Comparison between the model with and without ice”. The data set contains both an area with open water and an area with sea ice. Some of the area containing open water is covered by a big cloud.
The ice concentration for the data set has been calculated with our algorithm and with the NASA Team Sea Ice Algorithm, and the result can be seen in Figure 4-28. In Figure 4-29 is the standard deviation of the estimated ice concentration by our algorithm showed.
When looking at the estimated ice concentrations it can be seen, that the NASA team algorithm estimates a lower concentration than our algorithm over the ice covered area. The ice concentration over this area is expected to be 1, but when the truth concentration is not known exactly, it is not really possible to judge which of the algorithms gives the most correct ice concentration. On the other hand over the open water area the ice concentration is well known to be 0. When looking at the graphs it can be seen that our algorithm gives the most correct ice concentration. This is particularly clear in the area with the big cloud, where the NASA Team Sea Ice Algorithm calculates ice concentrations as high as 0.5.

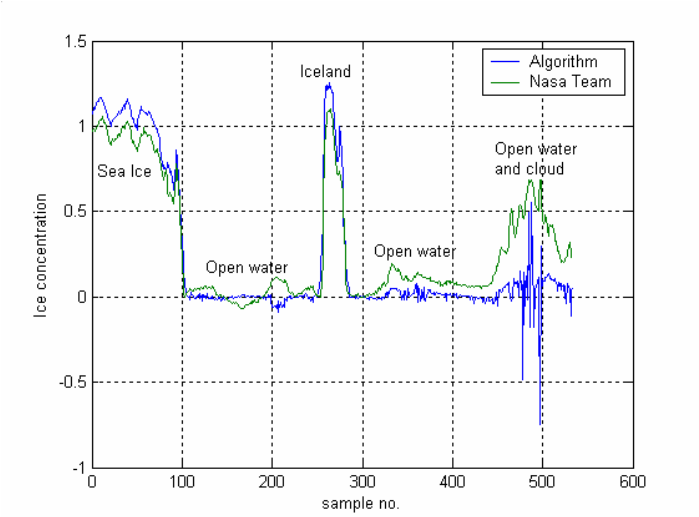

Figure 4-28 Ice concentrations from line of data at the 18th of November 2003.

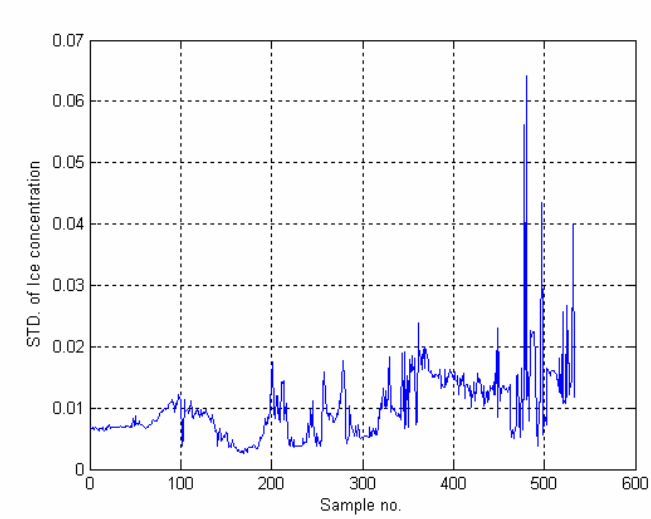

Figure 4-29 Standard deviation from our algorithm.

4.6.2 Time series

The places for the recording of the time series data are showed on the map on Figure 4-30. As examples have the open water areas 50, 51 and 52, the FY area 44 and the MY area 43 been used.

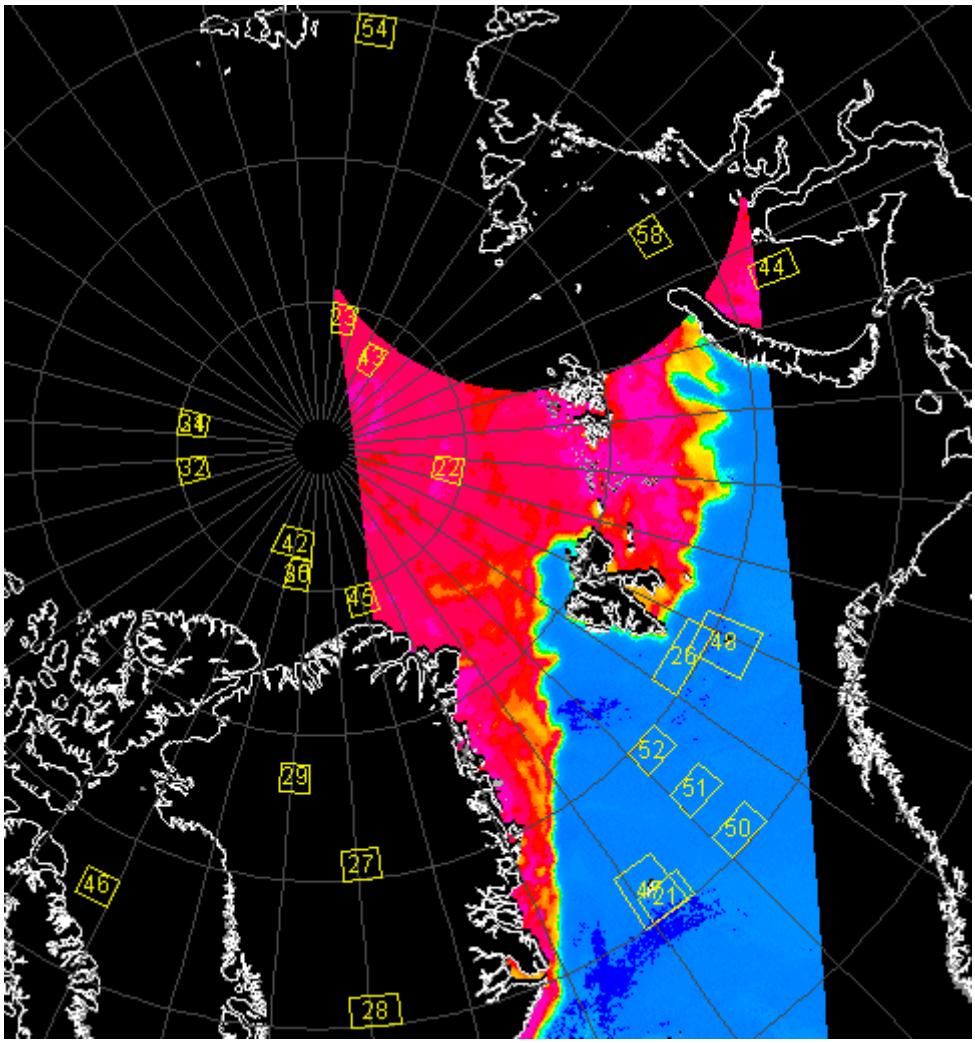

Figure 4-30 The Map shows the time series areas and the estimated ice concentration from the 18th of November 2003.

The results of the calculation over the open water area can be seen on Figure 4-31 to Figure 4-36, and a summary of the results are given in Table 4-1 to Table 4-3. For each of the 3 open water areas are 4 graphs showed. The first one shows the estimated ice concentration for the 2 algorithms. The second one shows the standard deviation for the estimated ice concentration from our algorithm. The last two graphs shows the calculated MY and FY concentration.

When looking at the graphs and the tables it can be seen, that our algorithm gives a better estimate of the ice concentration than the NASA Team Algorithm does, especially concerning the standard deviation. This is also the fact when looking at the estimation of the estimated ice concentration FY and MY ice. The standard deviations for our algorithm calculated from the time series (the one in the table) is, compared with the levels from the algorithm (the second graph), very high. This is because the standard deviation from our algorithm only represents how good the estimate is according to the model, and not how good the model actually is. Therefore the difference between the two standard deviations is a measure of how good the model actually is compared to real life.

When comparing the results form the three open water data set it can be seen that the standard deviation from the time series decreases the further north the data has been

collected, this is due to the lower temperature and thereby the lower amount of liquid water the further north one comes.

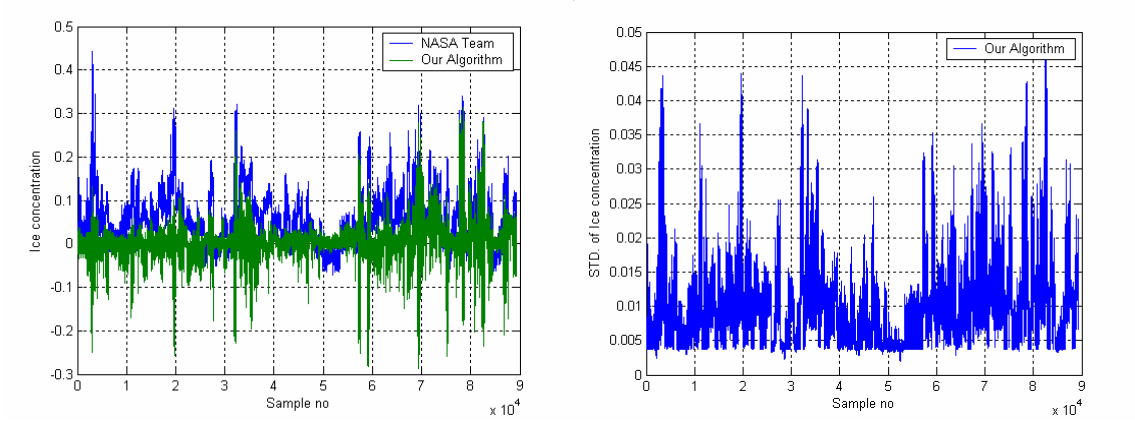

Figure 4-31 The left graph shows the total sea ice concentration for area 50, and the right graph shows the standard deviation from the estimation of the ice concentration by our algorithm.

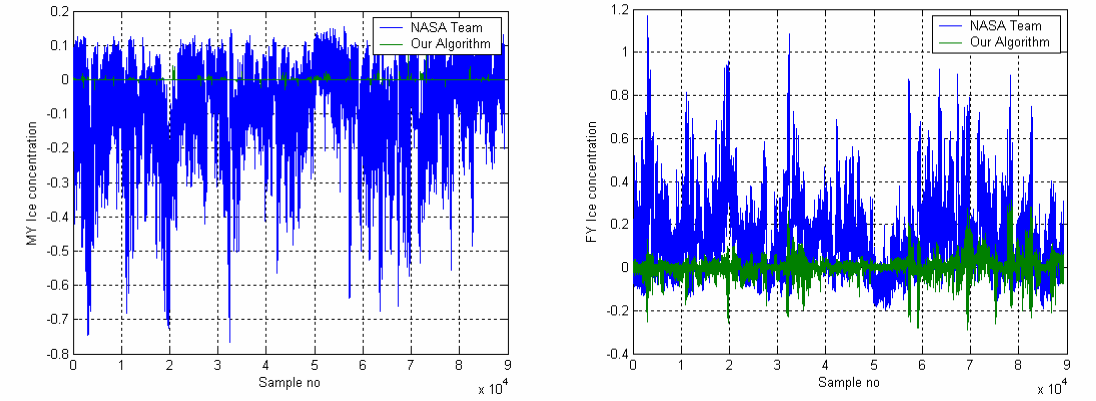

Figure 4-32 The left graph shows the MY ice concentration and the right graph shows the FY ice concentration for area 50.

	Total ice concentration		FY ice concentration		MY ice concentration	
	Mean	Std.	Mean	Std.	Mean	Std.
Our algorithm	0.0123	0.0405	0.0122	0.0404	0.0001	0.0015
NASA Team	0.0636	0.0614	0.1359	0.1648	-0.0722	0.1206

Table 4-3 The table shows the mean and standard deviation for each algorithm for area 50.

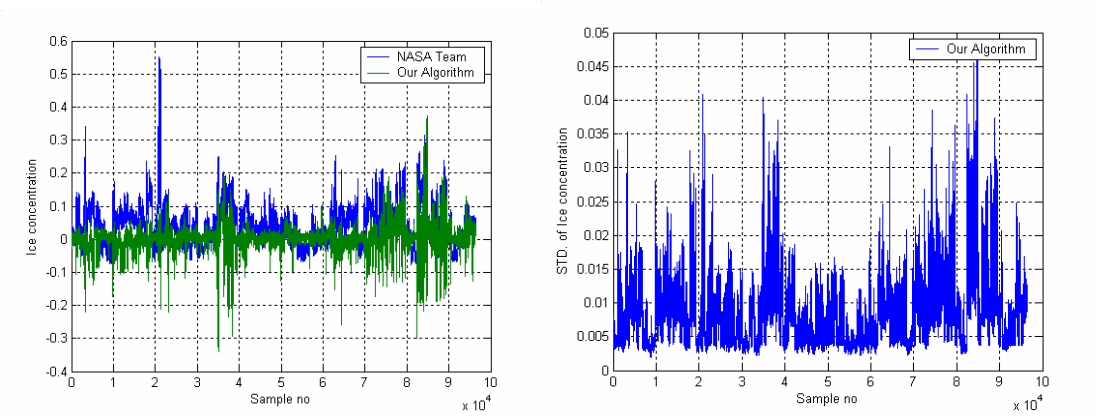

Figure 4-33 The graph shows the total sea ice concentration for area 51. The right graph shows the standard deviation of the ice concentration estimated by our algorithm.

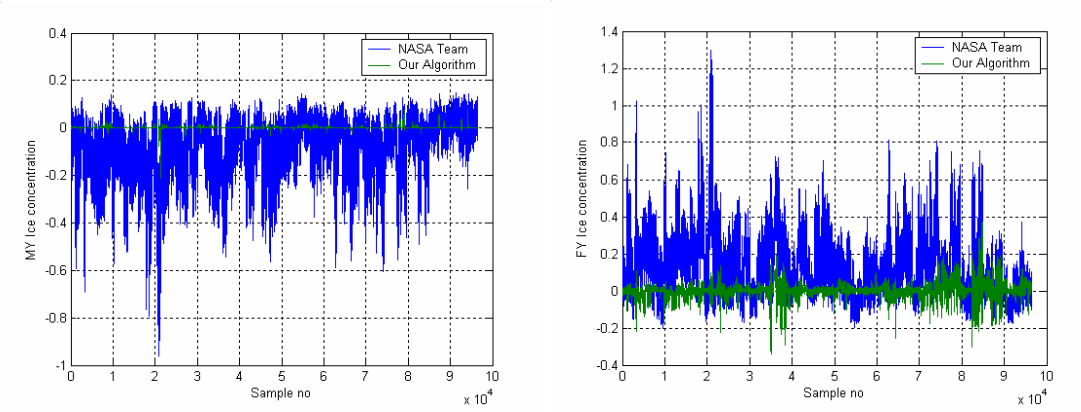

Figure 4-34 The left graph shows the MY ice concentration and the right graph shows the FY ice concentration for area 51.

	Total ice concentration		FY ice concentration		MY ice concentration	
	Mean	Std.	Mean	Std.	Mean	Std.
Our algorithm	0.0088	0.0391	0.0001	0.0042	0.0087	0.0388
NASA Team	0.0527	0.0626	-0.0793	0.1186	0.1320	0.1597

Table 4-4 The table shows the mean and standard deviation for each algorithm for area 51.

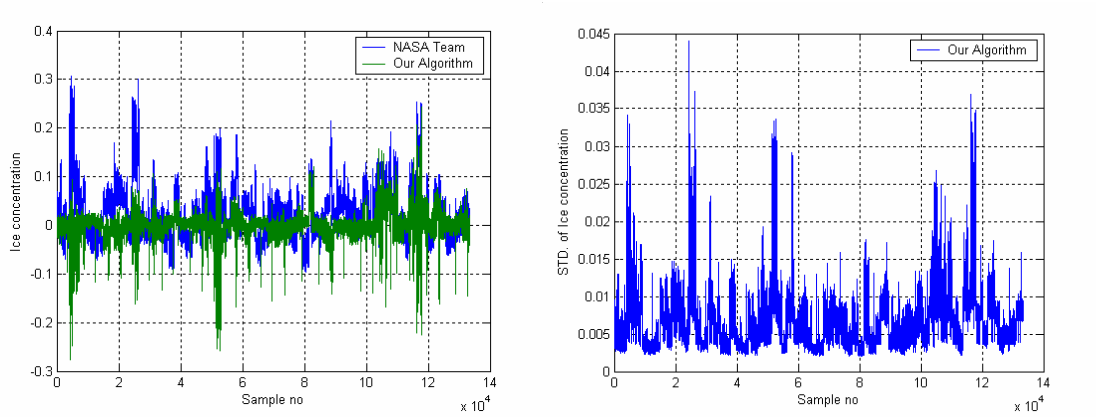

Figure 4-35 The graph shows the total sea ice concentration for area 52. The right graph shows the standard deviation of the ice concentration estimated by our algorithm.

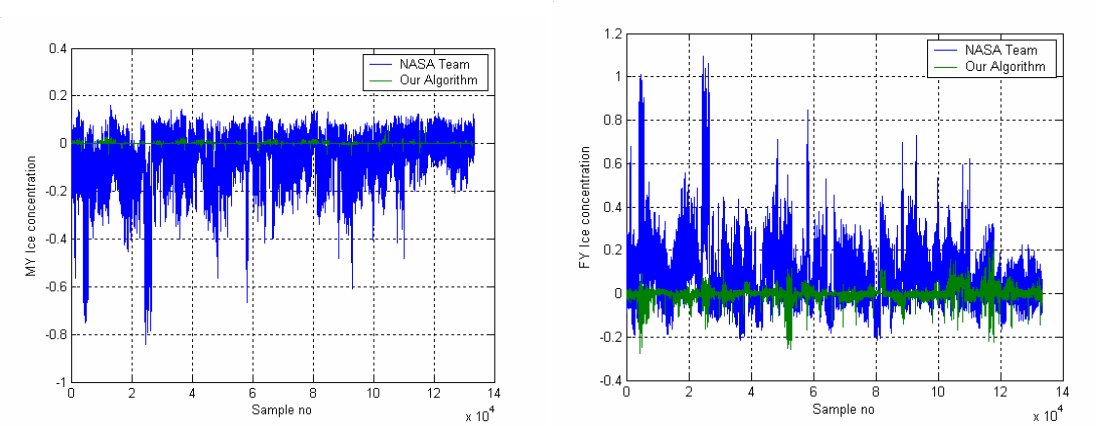

Figure 4-36 The left graph shows the MY ice concentration and the right graph shows the FY ice concentration for area 52.

	Total ice concentration		FY ice concentration		MY ice concentration	
	Mean	Std.	Mean	Std.	Mean	Std.
Our algorithm	0.0018	0.0274	0.0013	0.0269	0.0005	0.0028
NASA Team	0.0274	0.0509	0.0836	0.1302	-0.0563	0.0976

Table 4-5 The table shows the mean and standard deviation for each algorithm for area 52.

In Table 4-6 to Table 4-8 the results for 3 FY areas are showed, and in Table 4-9 and Table 4-10 the results for 2 MY areas are showed. When looking at the results in the tables, it can be seen, that our algorithm always estimates the highest ice concentration and often an ice concentration, which is higher than 1. Furthermore our algorithm estimates more MY ice than the NASA Team algorithm and less FY ice than the NASA Team algorithm. This indicates that the emissivities used in our algorithm are not fully correct, so this might be a subject for further investigations. The standard deviations obtained in the examples are very close to each other for the two algorithms, and thereby indicates that they probably represents some actual variations in the ice concentration.

	Total ice concentration		FY ice concentration		MY ice concentration	
	Mean	Std.	Mean	Std.	Mean	Std.
Our algorithm	1.0726	0.0423	0.3198	0.2321	0.7528	0.2081
NASA Team	0.9797	0.0419	0.8302	0.0997	0.1225	0.0888

Table 4-6 The table shows the mean and standard deviation for each algorithm for area 54 (FY area).

	Total ice concentration		FY ice concentration		MY ice concentration	
	Mean	Std.	Mean	Std.	Mean	Std.
Our algorithm	1.0166	0.1528	0.6524	0.3380	0.3642	0.2878
NASA Team	0.8646	0.1161	0.8177	0.1683	0.0428	0.0780

Table 4-7 The table shows the mean and standard deviation for each algorithm for area 44 (FY area).

	Total ice concentration		FY ice concentration		MY ice concentration	
	Mean	Std.	Mean	Std.	Mean	Std.
Our algorithm	0.9981	0.1273	0.6806	0.2960	0.3175	0.2801
NASA Team	0.8333	0.1214	0.7157	0.1586	0.1177	0.0701

Table 4-8 The table shows the mean and standard deviation for each algorithm for area 46 (FY area).

	Total ice concentration		FY ice concentration		MY ice concentration	
	Mean	Std.	Mean	Std.	Mean	Std.
Our algorithm	1.0152	0.0673	0.2034	0.1515	0.8118	0.1095
NASA Team	0.9220	0.0599	0.3179	0.1214	0.6041	0.0987

Table 4-9 The table shows the mean and standard deviation for each algorithm for area 23 (MY area).

	Total ice concentration		FY ice concentration		MY ice concentration	
	Mean	Std.	Mean	Std.	Mean	Std.
Our algorithm	1.0337	0.0421	0.1193	0.1132	0.9144	0.0964
NASA Team	0.9527	0.0492	0.3853	0.0911	0.5674	0.0782

Table 4-10 The table shows the mean and standard deviation for each algorithm for area 43 (MY area).

5 Examples

In this chapter, 4 examples of the use of the ice algorithm are described. The first three examples are from stable periods. This means periods where the microwave signature of the sea ice is stable, which is the case during winter time, when the temperature is low. The examples are from the 20th of March 2003 at 03:58, the 15th of November 2003 at 03:59 and at the 18th of November 2003 at 04:30.

The last of the 4 examples is from the 27th of October 2003 at 03:28, and is from an unstable period, where the microwave signature of the sea ice varies, because the temperature is still quite high and the ice is in the beginning of its formation period.

The time of the satellite passages given above is the equatorial crossing time. The satellite passages used as examples here are all ascending passages and only include data north of 40^0. Therefore the times given above are not the exact times for the data - the real time of the measurements are 10 to 25 minutes before the equatorial crossing time.

The results of the 4 examples are shown in the sections 5.2 to 5.5. In each of the sections an IR image of the area at about the same time as the AMSR satellite pass is shown as the first figure. Then there are two images (in one figure) for each of the estimated geophysical parameters one for the estimated parameter, and one for the standard deviation of the estimated parameter. The results of each of the examples will not be analyzed separately in each section. In stead the over all estimation of the geophysical parameters will be analyzed in section 5.6 “Summary of the results of the examples “.

5.1 Masking of the data

Before doing any calculations the raw AMSR data are masked using a 7.5 kilometer land mask in order to avoid meaningless retrieval computations over land where the forward model is not valid. If any land is present within 11.25 kilometers of an AMSR sample point, that AMSR sample will be removed from the processing.
After the retrieval of the geophysical parameters has taken place some of the estimated parameters are masked. Estimated parameters unlikely to be correct are removed so that they are not showed in the images from the 4 examples. The condition of the masking and the action taken from the mask is shown in Table 5-1.

Estimated parameter	***Masking conditions***	***Action***
Wind speed, W, [m/s]	If $C_{is}>0.5$	Pixel black
Open water sea surface temperature, T_{ow}, [K]	If $C>0.2$ If Test_value>4 If $T_{ow}>300$	Pixel black Pixel black Pixel black
Sea ice surface temperature, T_{is}, [K]	If $C<0.2$ If std(T_{is})>1.0	Pixel black Pixel black
Multi Year Ice Fraction, F_{MY}	If std(F_{MY})>0.15	Pixel black

Table 5-1 The table shows the masking conditions and the action taken by the mask for the images of the estimated geophysical parameters.

When looking at the estimated parameters, some of the parameters (e.g. the sea surface temperature at Figure 5-14) are always estimated wrongly in the left side of the orbit. The error in the estimated parameters does not occur because of an error in the retrieval algorithm. But the error relates back to an error in the measured low frequency brightness temperature, because the spacecraft body slightly interferes with the field of view. We have not looked further in to the problem, but it can be solved rather easily by removing some of the first samples in each AMSR scan.

5.2 Example from the 20th of March 2003 –stable period

In this section the results of the estimated geophysical parameters are showed for the AMSR satellite passage at the 20th of March 2003. The satellite passage was a descending orbit and the equator crossing time was at 03:59.

As a reference an IR image of the area at 03:45 is showed at Figure 5-1. On this image one can se, that the orbit contains data measured over a big cloud in the southwestern part of the orbit. These data probably contain a high level of water vapor, liquid water, and maybe also a lot of wind. In the northern part of the orbit there is a somewhat smaller formation of clouds. The important thing about these clouds is that they start over the open water and then continues over the ice edge and further on to cover the actual ice surface. This continuity of the clouds over the different surface types, one should be able to recognize in the retrieved geophysical parameters of water.

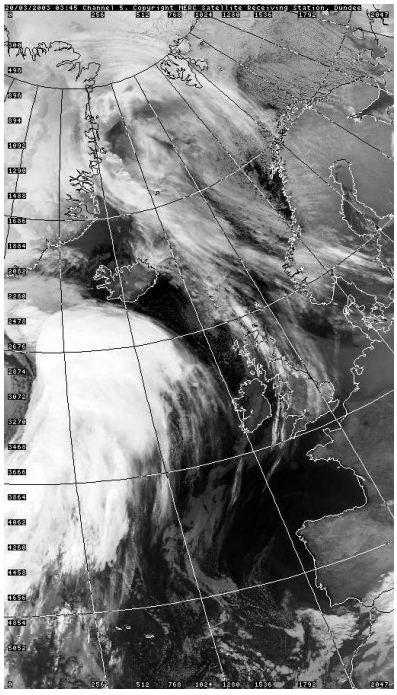

Figure 5-1 IR image from the 20th of March 2003 at 03:45

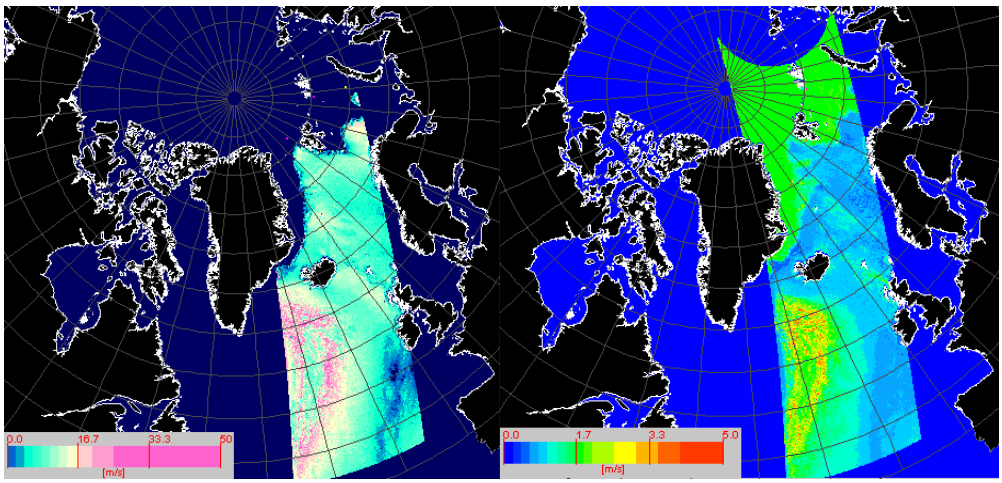

Figure 5-2 The left image shows the estimated wind speed, and the right image shows the standard deviation of the estimated wind speed from the 20th of March 2003 at 03:59.

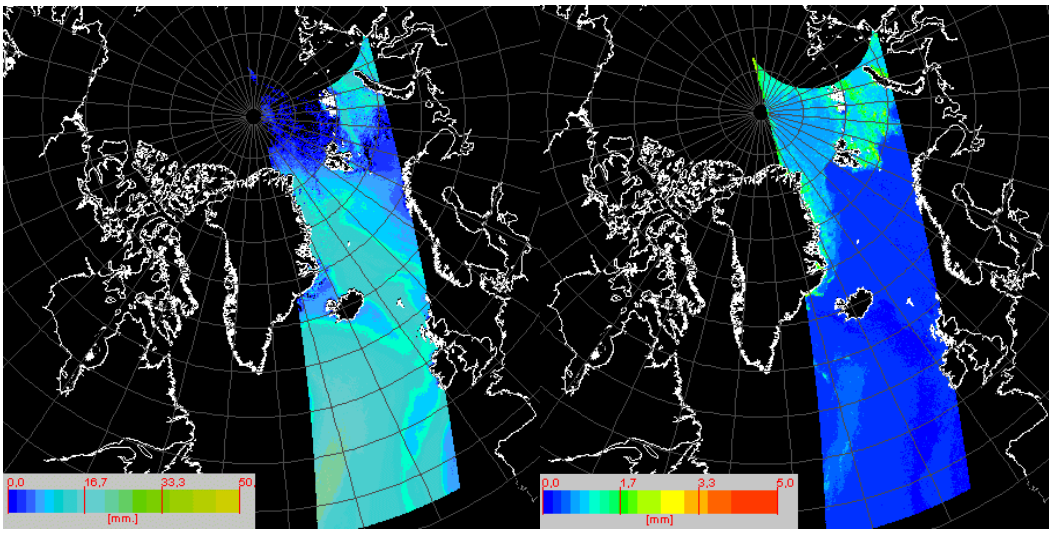

Figure 5-3 The left image shows the estimated water vapor, and the right image shows the standard deviation of the estimated water vapor from the 20th of March 2003 at 03:59.

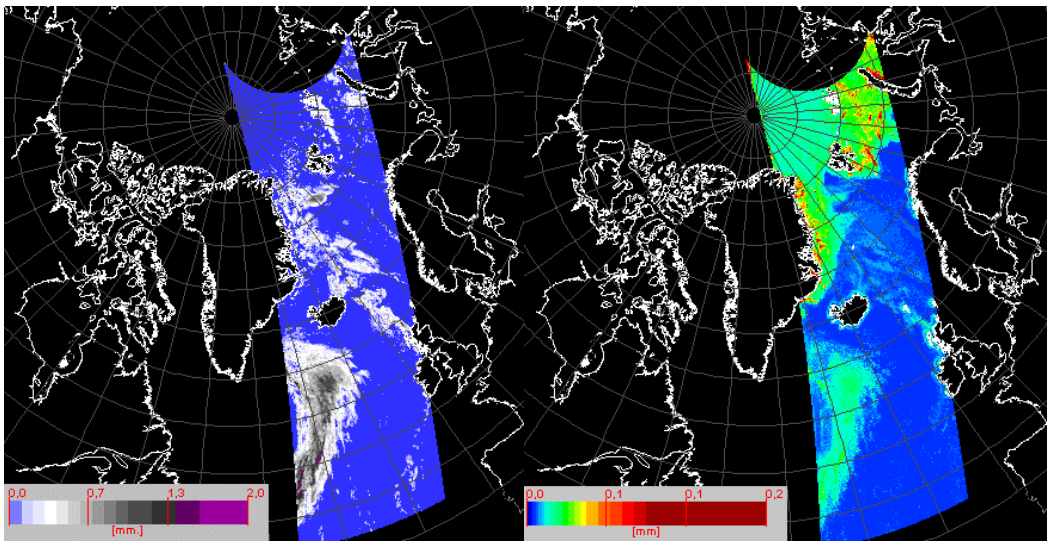

Figure 5-4 The left image shows the estimated liquid water, and the right image shows the standard deviation of the estimated water vapor from the 20th of March 2003 at 03:59.

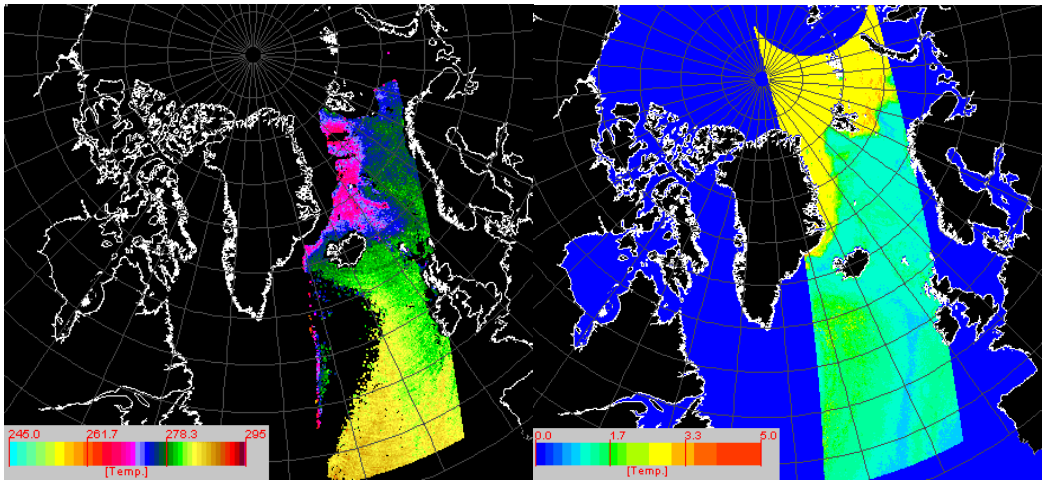

Figure 5-5 The left image shows the estimated open water sea surface temperature, and the right image shows the standard deviation of the estimated open water sea surface temperature from the 20th of March 2003 at 03:59.

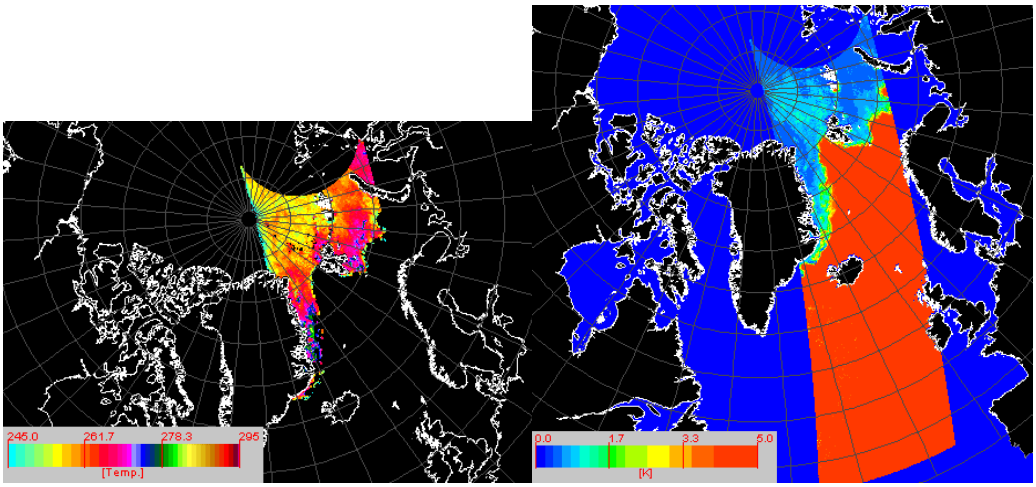

Figure 5-6 The left image shows the estimated surface temperature of the sea ice, and the right image shows the standard deviation of the estimated surface temperature of the sea ice from the 20th of March 2003 at 03:59.

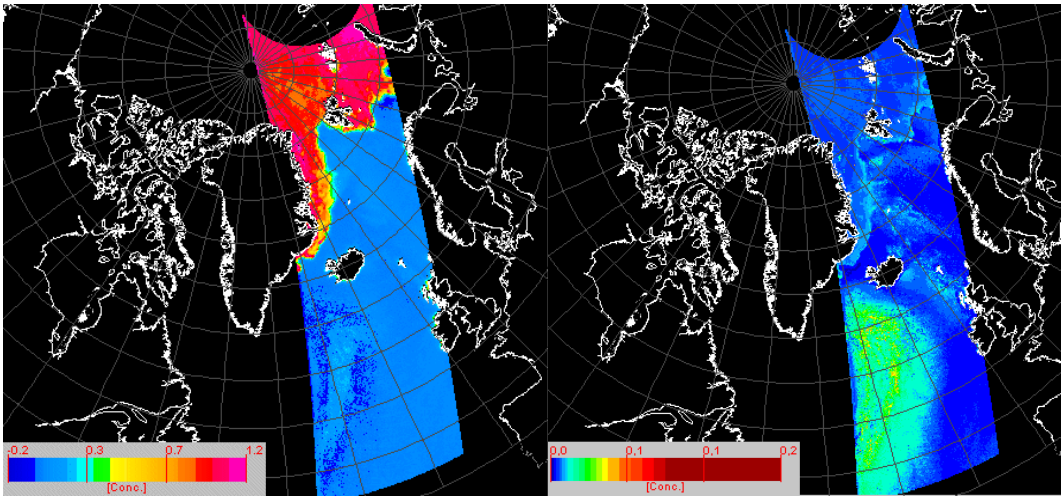

Figure 5-7 The left image shows the estimated sea ice concentration, and the right image shows the standard deviation of the estimated sea ice concentration from the 20th of March 2003 at 03:59.

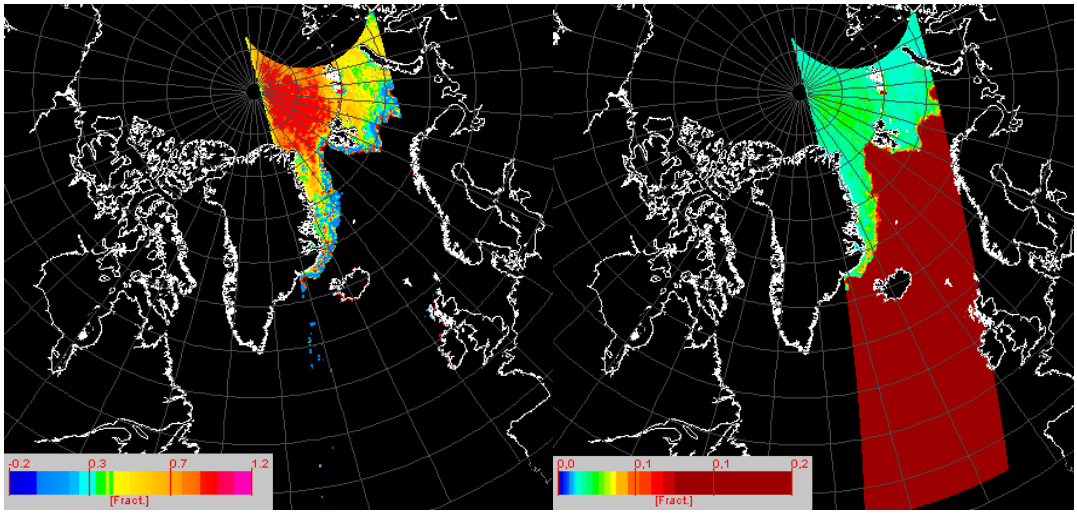

Figure 5-8 The left image shows the estimated multi year ice fraction, and the right image shows the standard deviation of the estimated multi year ice fraction from the 20th of March 2003 at 03:59.

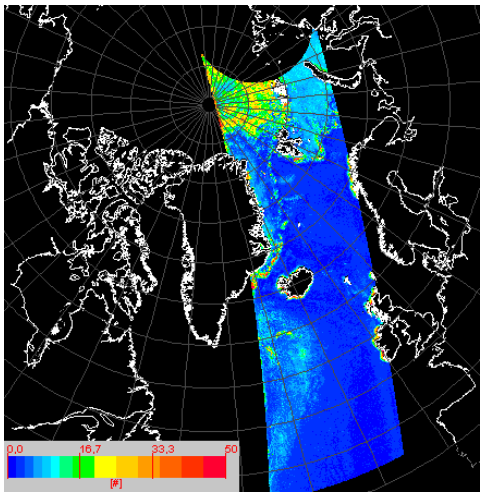

Figure 5-9 Test value from the 20th of March 2003 at 03:59.

5.3 Example from the 15th of November 2003 - Stable period

In this section the results of the estimated geophysical parameters are showed for the AMSR satellite passage at the 15th of November 2003. The satellite passage was a descending orbit and the equator crossing time was at 03:59.
As a reference an IR image of the area at 03:58 is showed at Figure 5-10. On this image it can be seen that the orbit contains data measured mainly over open water with only a small amount of clouds.

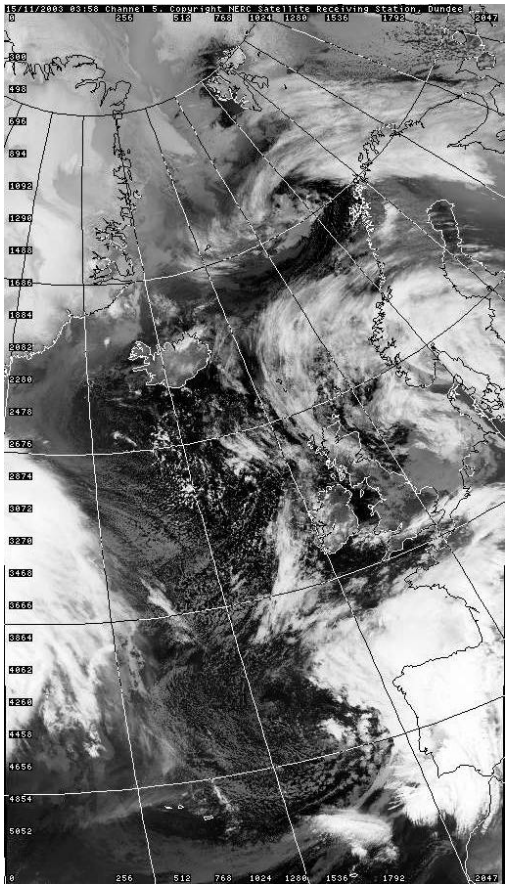

Figure 5-10 IR image from the 15th of November 2003 at 03:58

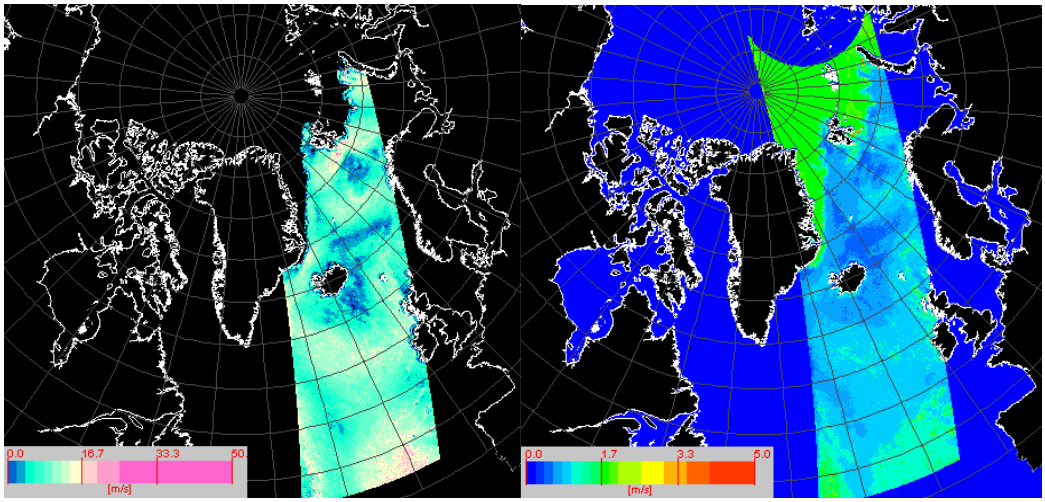

Figure 5-11 The left image shows the estimated wind speed, and the right image shows the standard deviation of the estimated wind speed from the 15th of November 2003 at 03:59.

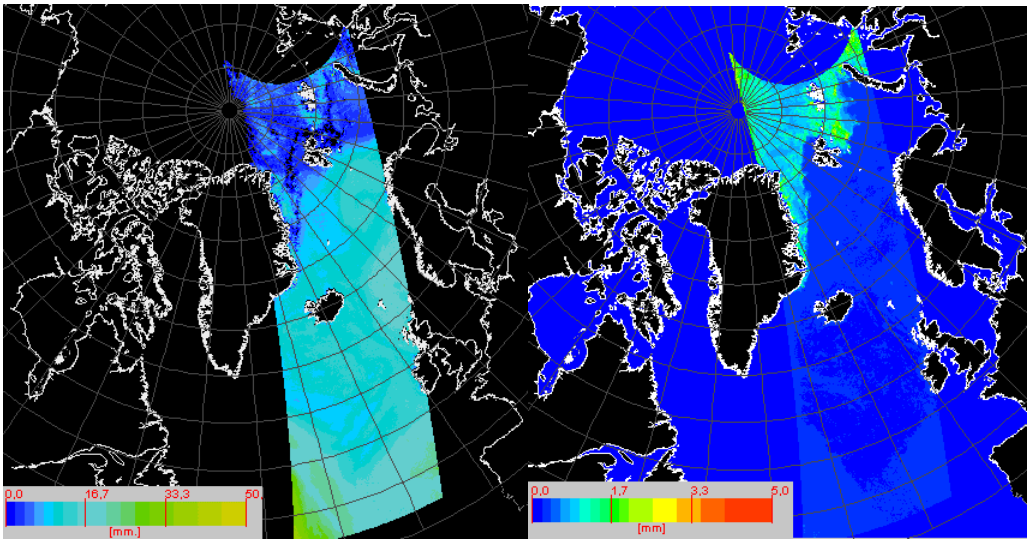

Figure 5-12 The left image shows the estimated water vapor, and the right image shows the standard deviation of the estimated water vapor from the 15th of November 2003 at 03:59.

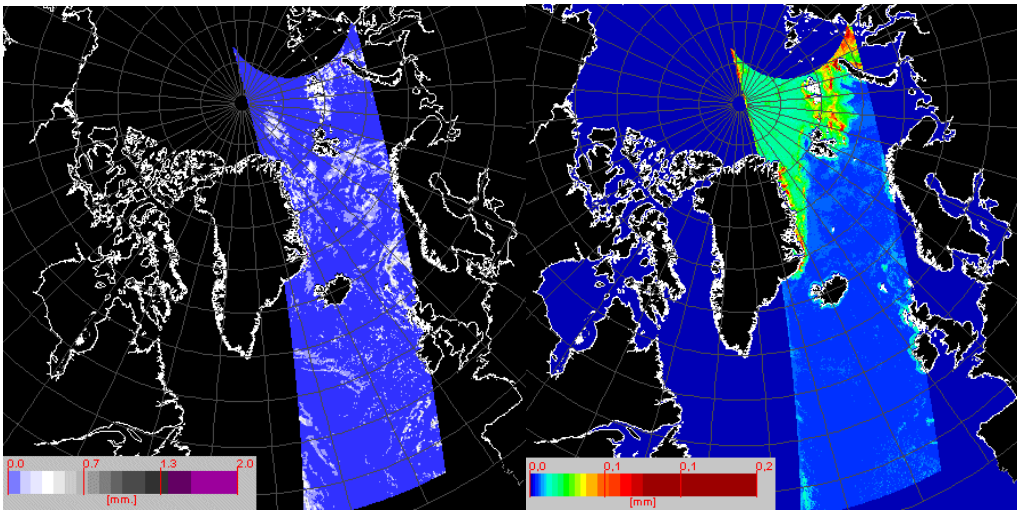

Figure 5-13 The left image shows the estimated liquid water, and the right image shows the standard deviation of the estimated water vapor from the 15th of November 2003 at 03:59.

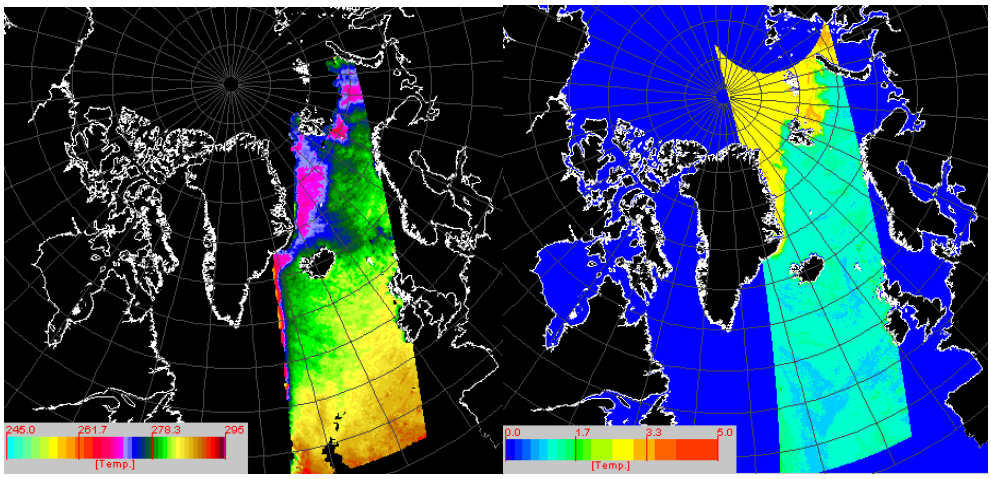

Figure 5-14 The left image shows the estimated open water sea surface temperature, and the right image shows the standard deviation of the estimated open water sea surface temperature from the 15th of November 2003 at 03:59.

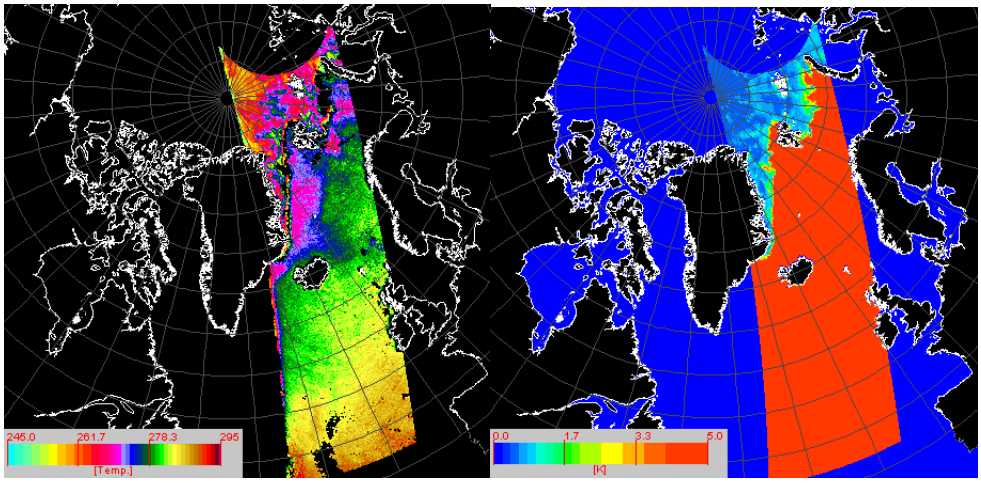

Figure 5-15 The left image is a combined image of the estimated sea ice temperature and the estimated open water sea surface temperature (same as on Figure 5-14), the right image shows the standard deviation of the estimated sea ice temperature from the 15th of November 2003 at 03:59.

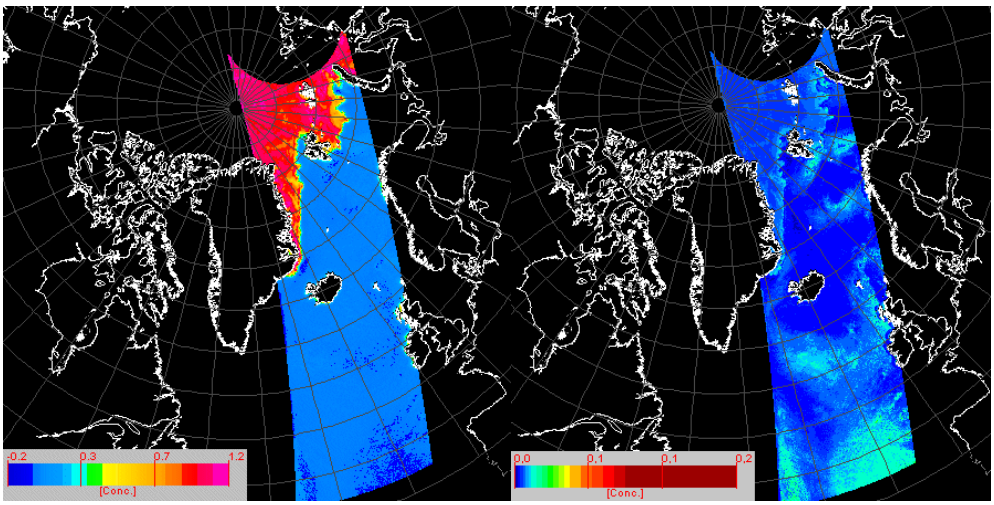

Figure 5-16 The left image shows the estimated sea ice concentration, and the right image shows the standard deviation of the estimated sea surface temperature from the 15th of November 2003 at 03:59.

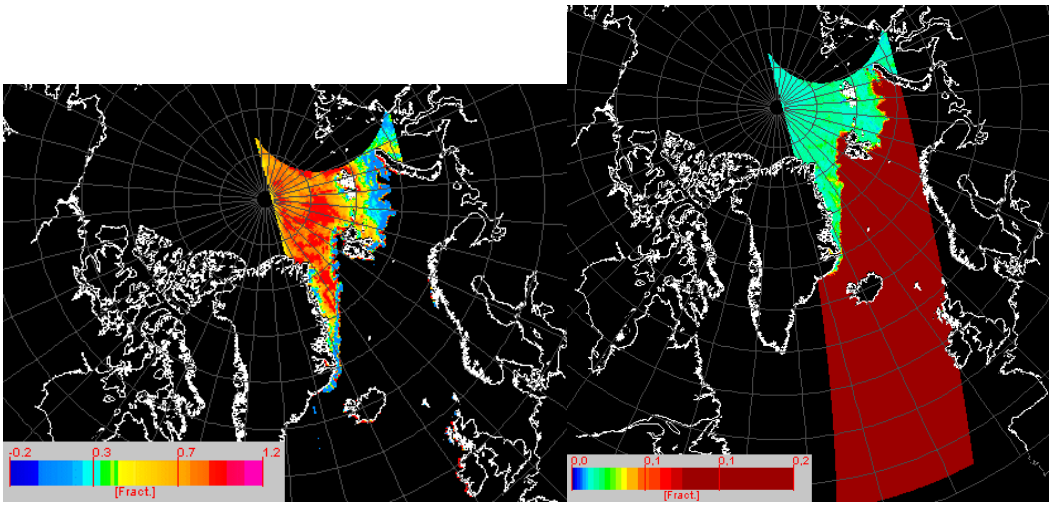

Figure 5-17 The left image shows the estimated Multi year ice fraction, and the right image shows the standard deviation of the estimated multi year ice fraction from the 15th of November 2003 at 03:59.

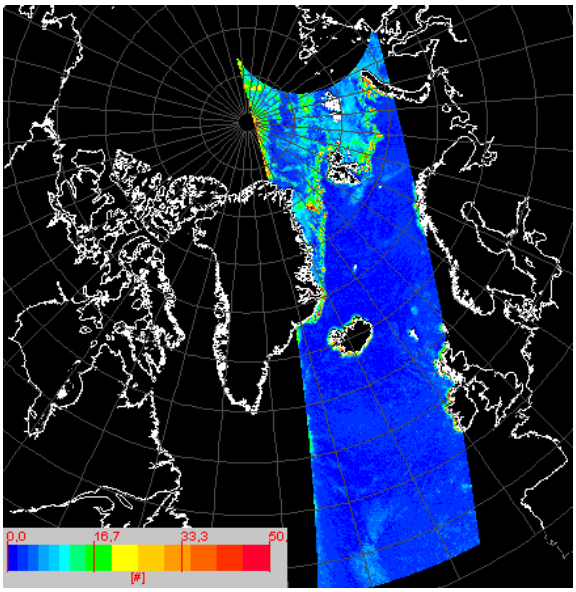

Figure 5-18 Test value from the 15th of November 2003 at 03:59

5.4 Example from the 18th of November 2003 – Stable period

In this section the results of the estimated geophysical parameters are showed for the AMSR satellite passage at the 18th of November 2003. The satellite passage was a descending orbit and the equator crossing time was at 04:30.
As a reference an IR image of the area at 03:24 is showed at Figure 5-19. On this image it can be seen, that this orbit contains data measured over some big clouds in the southern part of the orbit, which probably contain a high level of water vapor, liquid water and maybe also some wind.

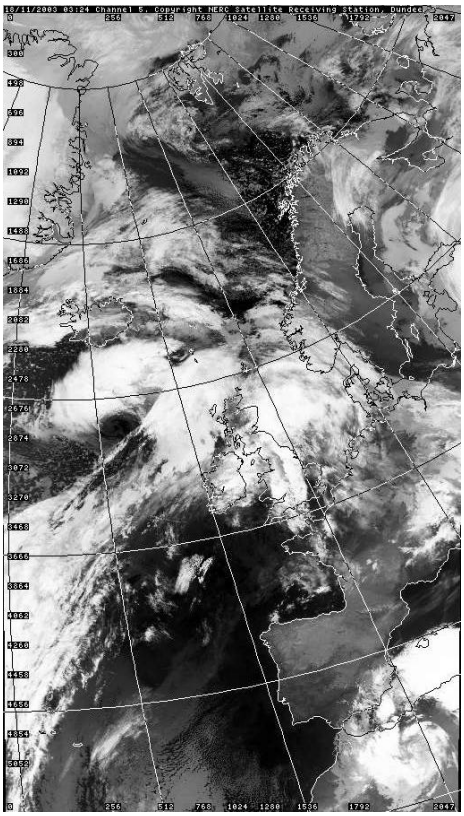

Figure 5-19 IR image from the 18th of November 2003 at 03:24

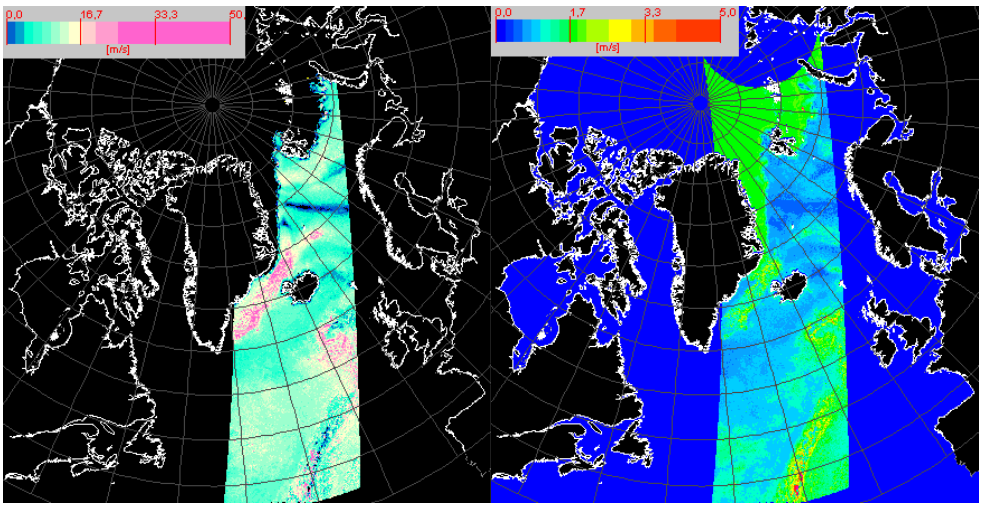

Figure 5-20 The left image shows the estimated wind speed, and the right image shows the standard deviation of the estimated wind speed from the 18th of November 2003 at 04:30.

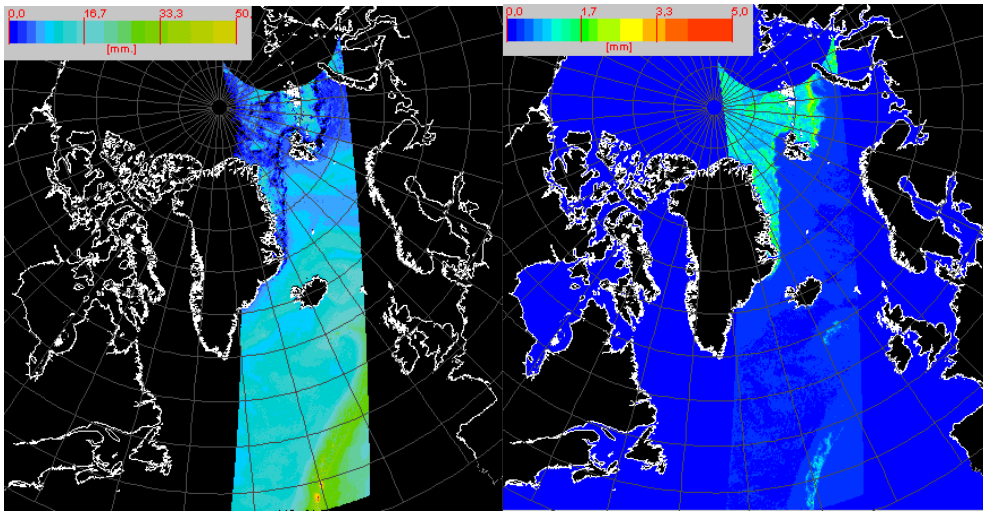

Figure 5-21 The left image shows the estimated water vapor, and the right image shows the standard deviation of the estimated water vapor from the 18th of November 2003 at 04:30.

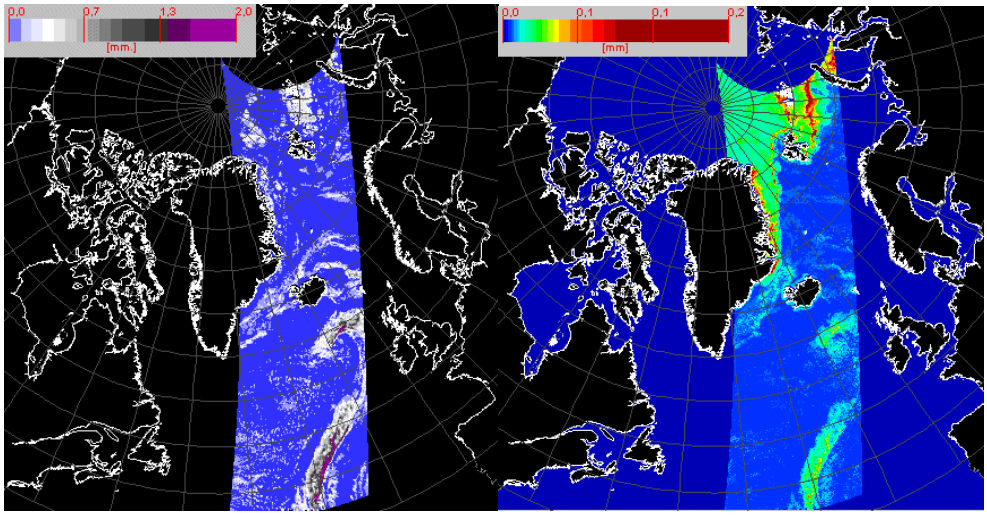

Figure 5-22 The left image shows the estimated liquid water, and the right image shows the standard deviation of the estimated water vapor from the 18th of November 2003 at 04:30.

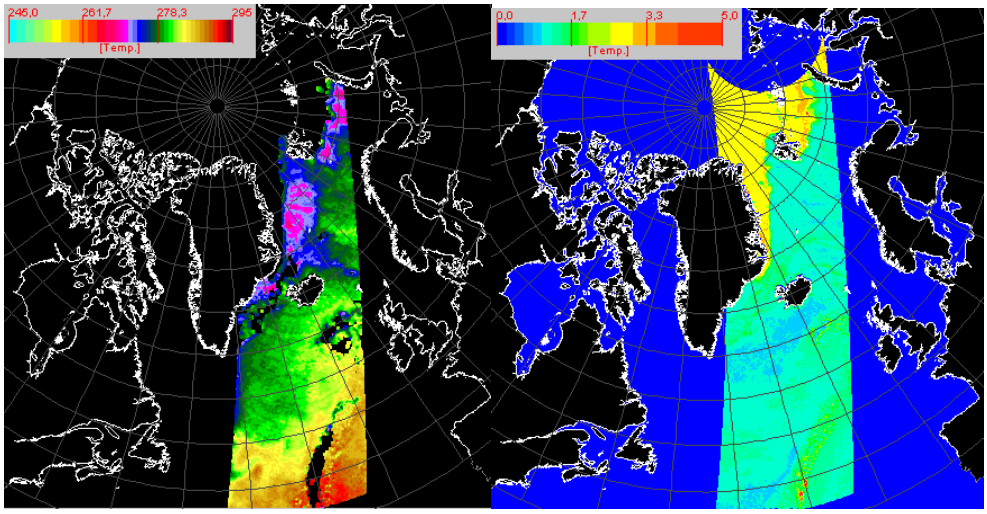

Figure 5-23 The left image shows the estimated open water sea surface temperature, and the right image shows the standard deviation of the estimated open water sea surface temperature from the 18th of November 2003 at 04:30.

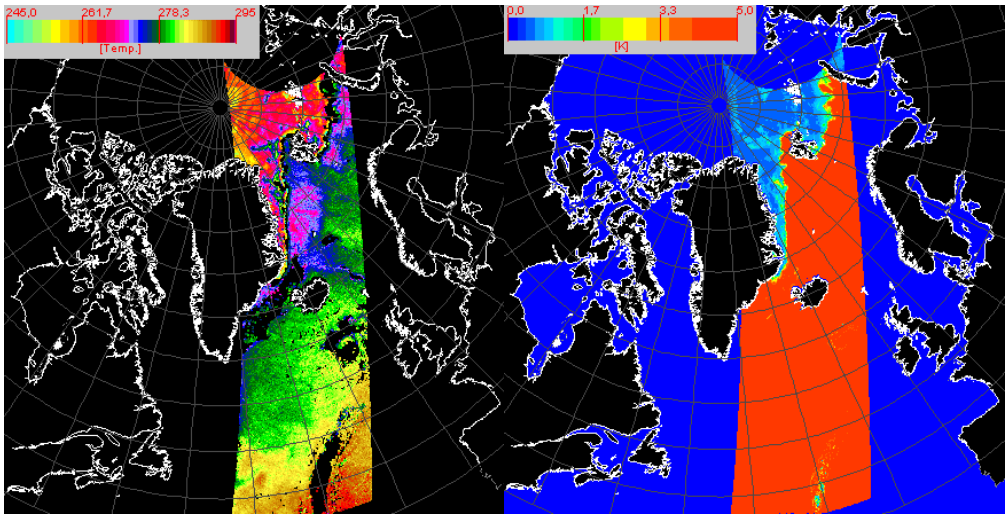

Figure 5-24 The left image is a combined image of the estimated sea ice temperature and open water sea surface temperature (same as on Figure 5-14), the right image shows the standard deviation of the estimated sea ice temperature from the 18th of November 2003 at 04:30.

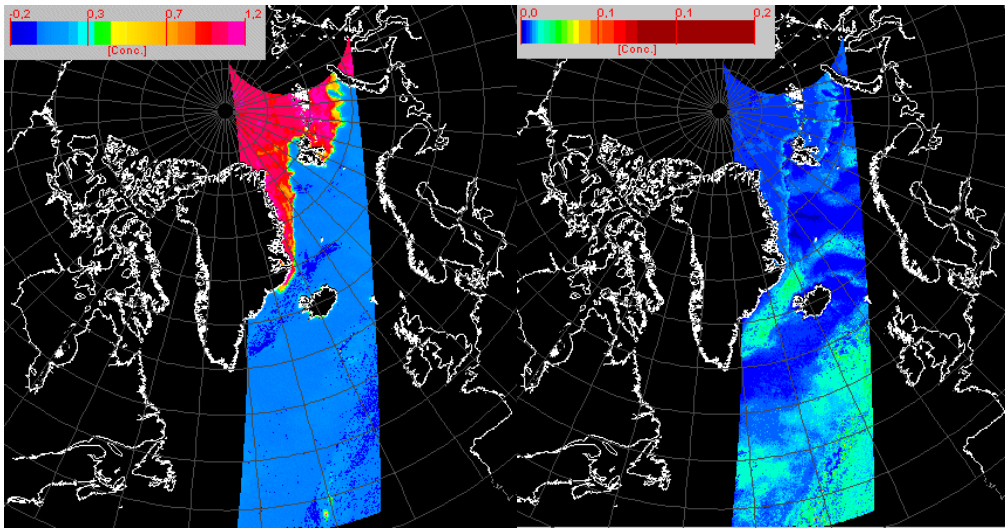

Figure 5-25 The left image shows the estimated sea ice concentration, and the right image shows the standard deviation of the sea surface temperature from the 18th of November 2003 at 04:30.

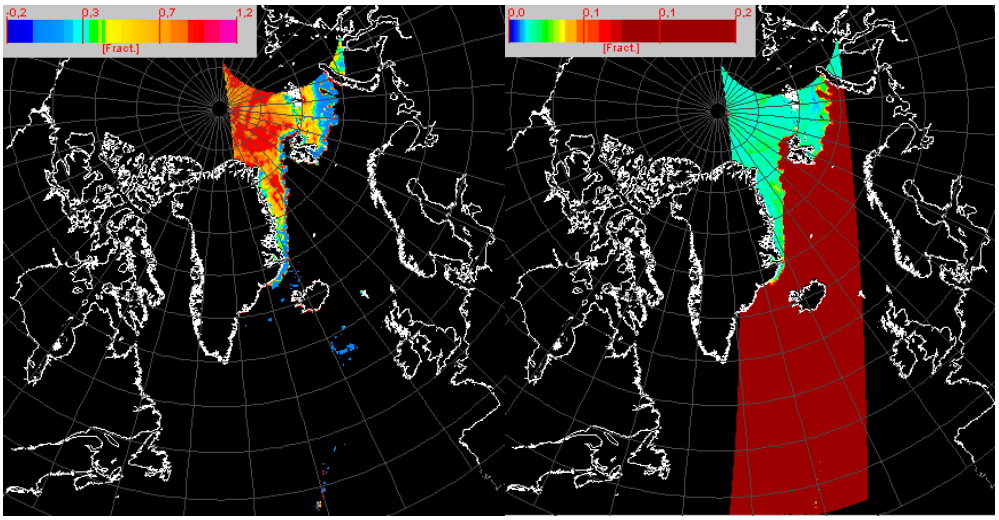

Figure 5-26 The left image shows the estimated Multi year ice fraction, and the right image shows the standard deviation of the multi year ice fraction from the 18th of November 2003 at 04:30.

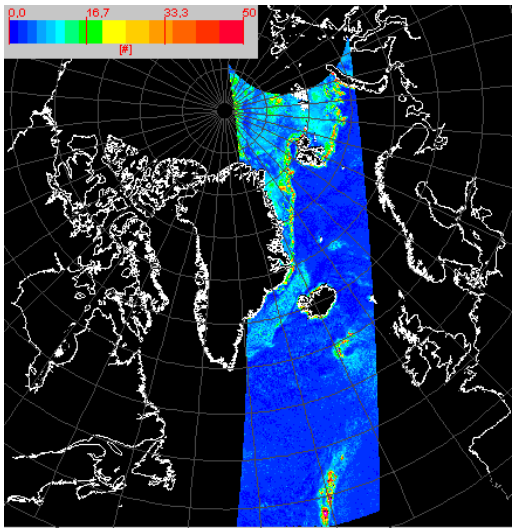

Figure 5-27 Test value from the 18th of November 2003 at 04:30.

5.5 Example from the 27th of October 2003 – Unstable period

In this section the results of the estimated geophysical parameters are showed for the AMSR satellite passage at the 27th of October 2003. The satellite passage was a descending orbit and the equator crossing time was at 03:28.

As a reference an IR image of the area at 04:12 is showed at Figure 5-28. On this image it can be seen that the orbit contains data measured over a big cloud in the northeastern part of the orbit. These data probably contain a high level of water vapor, liquid water and maybe also a lot of wind.

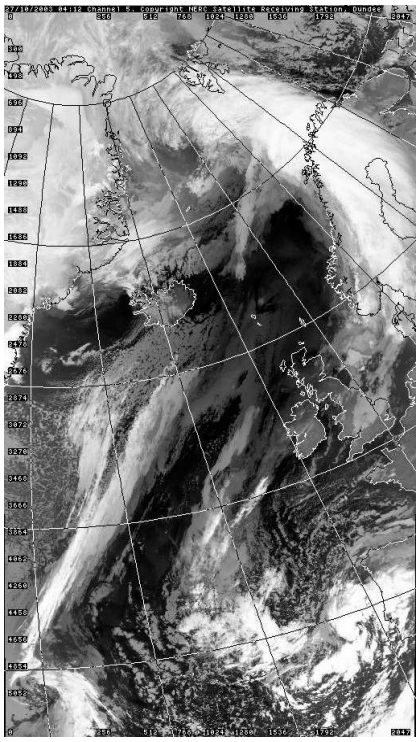

Figure 5-28 IR image from the 27th of October 2003 at 04:12

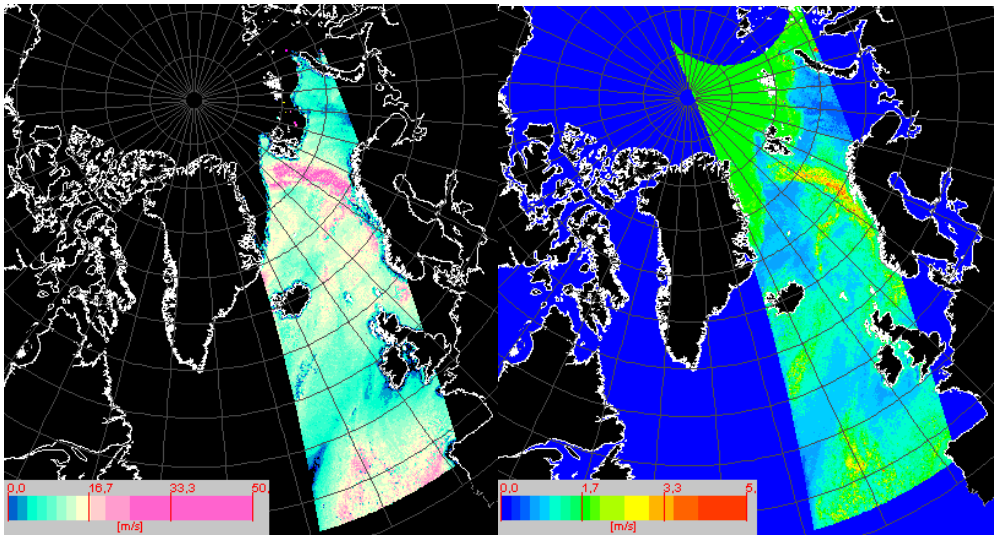

Figure 5-29 The left image shows the estimated wind speed, and the right image shows the standard deviation of the estimated wind speed from the 27th of October 2003 at 03:28.

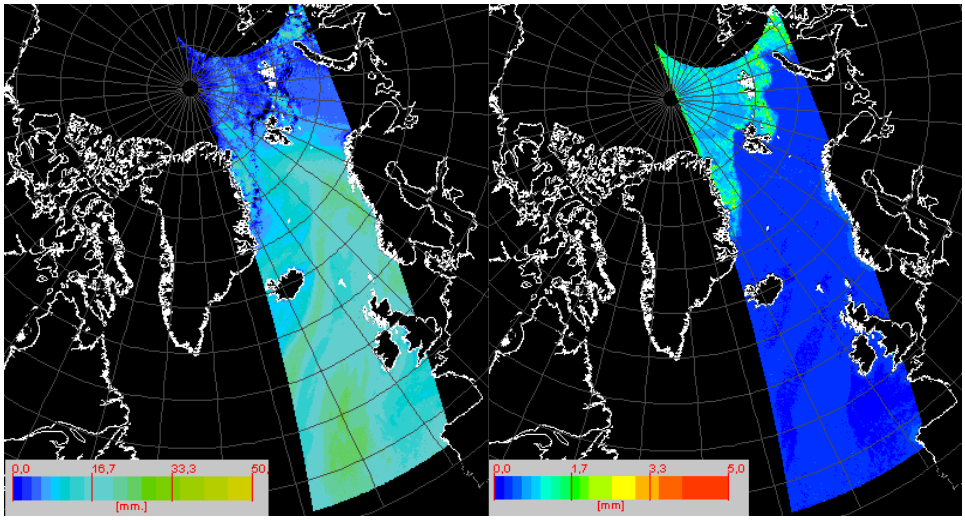

Figure 5-30 The left image shows the estimated water vapor, and the right image shows the standard deviation of the estimated water vapor from the 27th of October 2003 at 03:28.

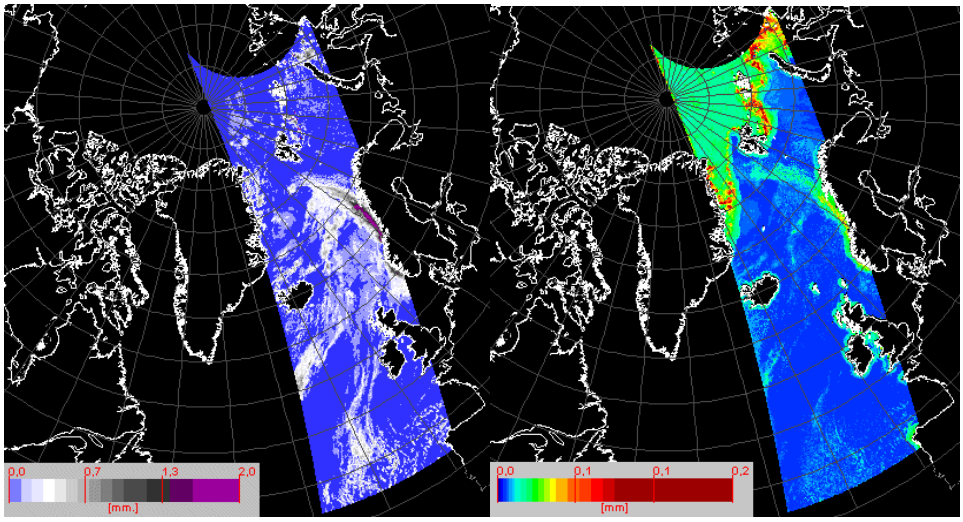

Figure 5-31 The left image shows the estimated liquid water, and the right image shows the standard deviation of the estimated liquid vapor from the 27th of October 2003 at 03:28.

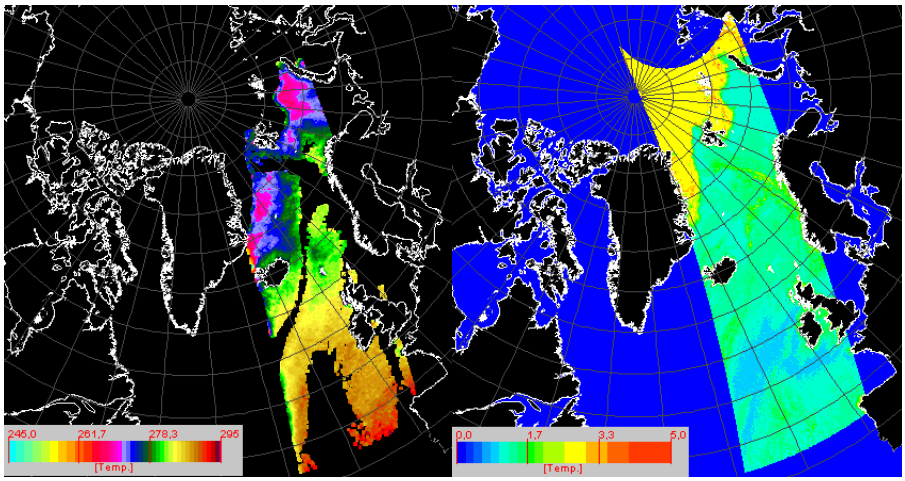

Figure 5-32 The left image shows the estimated open water sea surface temperature, and the right image shows the standard deviation of the estimated open water sea surface temperature from the 27th of October 2003 at 03:28.

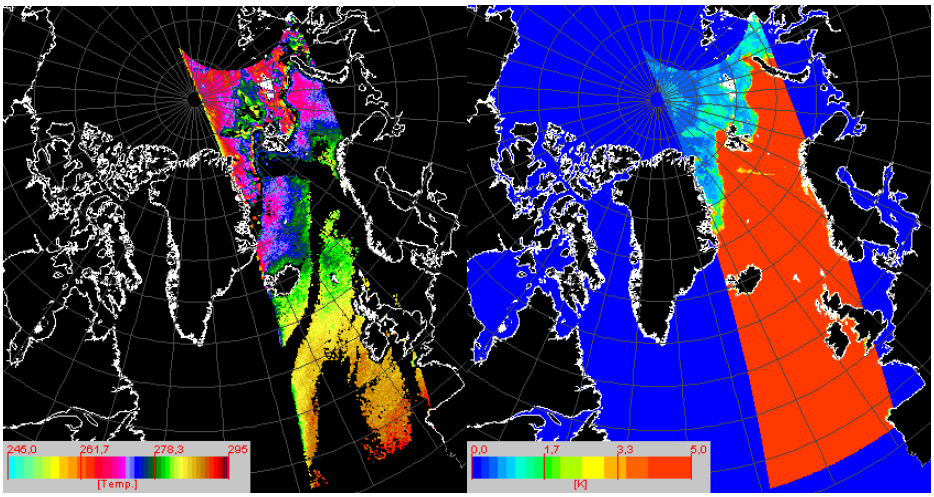

Figure 5-33 The left image is a combined image of the estimated sea ice temperature and the estimated open water sea surface temperature (same as on Figure 5-32), the right image shows the standard deviation of the estimated sea ice temperature from the 27th of October 2003 at 03:28.

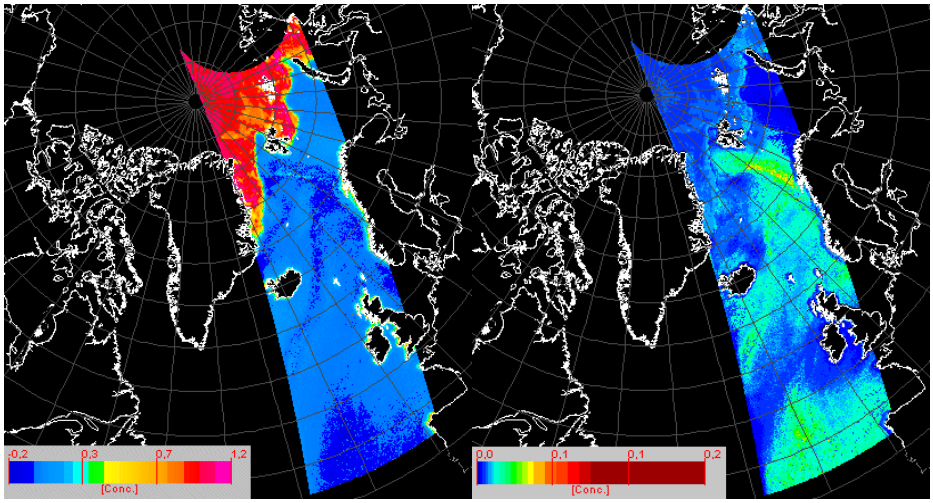

Figure 5-34 The left image shows the estimated sea ice concentration, and the right image shows the standard deviation of the estimated sea surface temperature from the 27th of October 2003 at 03:28.

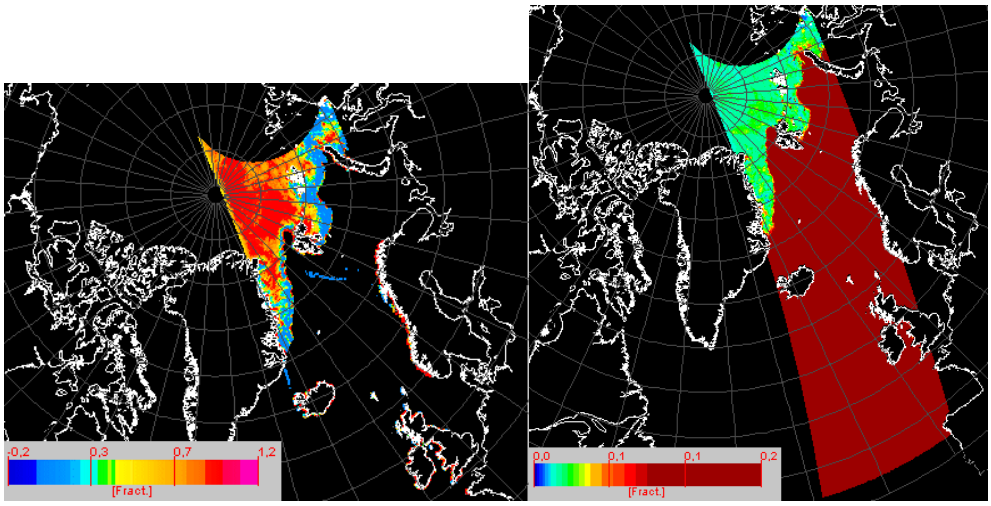

Figure 5-35 The left image shows the estimated Multi year ice fraction, and the right image shows the standard deviation of the estimated multi year ice fraction from the 27th of October 2003 at 03:28.

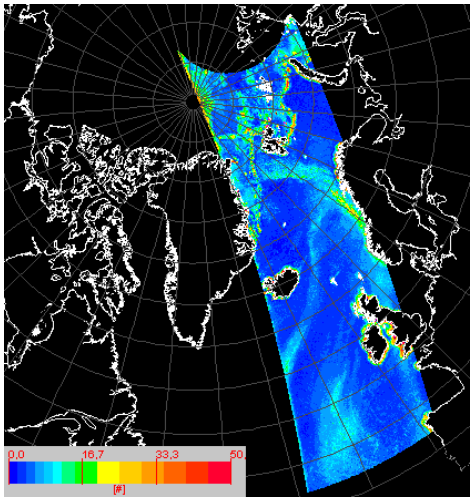

Figure 5-36 Test value from the 27th of October 2003 at 03:28.

5.6 Summary of the results of the examples

5.6.1 Wind speed

From the 4 examples it can be seen, that the wind speed can be estimated over the open water sea surface but not over the ice surface. A good example of the estimated wind speed can be seen on Figure 5-11 from the 15th of November 2003. On this figure one can see by comparing the estimated value with the standard deviation, that when a high value has been estimated for the wind speed, then the standard deviation is also high. Furthermore it can be noted, that the spatial patterns of the winds are as expected.
On some of the images of wind speed, it looks like, there are some strange phenomenons. An example is Figure 5-20 in the southeastern part of the image, where a very high wind speed has been estimated right beside a very low one. This is not likely to be correct so maybe the images of the wind speed should have been masked in order to remove these unlikely situations. The forward model does not include rain, and maybe the situation occurs because of interference from rain. Therefore it might be a good idea in the future to include some kind of a rain flag as a mask to the estimated wind speed.

5.6.2 Water vapor

When estimating the amount of integrated columnar water vapor it can be seen from the 4 examples, that water vapor can be estimated both over open water and over the sea ice surface. This is illustrated well on Figure 5-3 from the 20th of March 2003, where it also can be seen, that the standard deviation of the estimate increases over the ice surface. Furthermore the standard deviation also increases over open water, if larger amounts of water vapor occur in the atmosphere. This phenomenon can be seen in the results from the 18th of November 2003 on Figure 5-21 in the southeastern part of the orbit. In the images showing the estimated amounts of water vapor there are some areas which are back. This is not because the images have been masked, but because those pixels have a very low value, which is not included in the color scale.

5.6.3 Liquid water

The amount of the integrated columnar liquid water can, as with the water vapor, be estimated over the ice. This can be seen illustrated on Figure 5-4, where the estimated amount of liquid water is shown for the 20th of March 2003. The standard deviation of the estimate is in general low over open water and higher over ice. But if there is a high amount of liquid water in the atmosphere over the open water the standard deviation increases.
Over the ice surface there are some specific places where the standard deviation is higher than everywhere else over the ice surface. An example of this can be seen on Figure 5-13. If comparing this figure with the multi year ice fraction on Figure 5-17 one can see that the areas, which have a high standard deviation for the liquid water, are the same areas, which contains a high concentration of first year ice.

5.6.4 Surface temperature

As explained earlier 2 surface temperatures have been estimated one for the open water sea surface T_{ow} and one for the sea ice surface T_{is}. So in the examples there are two figures of the temperatures. The first one is always an image of the open water temperature and its standard deviation. The second figure is for two of the examples a figure of the sea ice temperature alone (e.g. Figure 5-6) and for two of the examples the second figure shows the entire surface temperature (combination of T_{ow} and T_{is} e.g. Figure 5-15). On the combined images one can see that the two temperatures do not fit exactly together, because there is a black line between the two surface types. This is because the temperatures are difficult to estimate – has a high standard deviation – when the two surface types are mixed, which is the case at the edge of the ice. Together with the combined image the standard deviation of the ice temperature is shown – not the combined standard deviation!
When looking at the open water temperature in Figure 5-5 one can see, that the temperature, as expected, is low in the north and increases toward the south. In the area north of Iceland and south of the ice edge it can be seen that the temperatures estimated are unrealistically low. This failure in the estimation has not been investigated further, but one has to look into this problem in the future. Another problem concerning the estimation of the open water temperature is the line of error estimates to the left in the image, which have been mentioned earlier. When looking at the image it can be seen that under the big cloud, which contains a lot of water, the test values were very high, and therefore the estimated temperatures were removed by the masking.
When considering the ice surface temperature for instant in Figure 5-6 it can be seen that the ice temperature, as expected, is higher in areas with FY ice than in areas with

MY ice. When considering the standard deviation it can be seen, that it has its highest values near the ice edge (when not considering the standard deviation over the open water sea surface). When considering the example from the unstable period in Figure 5-33 it can be seen, that the temperatures have been estimated to give some unrealistic values, and furthermore it can not be seen on the standard deviation, that the estimate is wrong, so this is one of the limitations of the method.

5.6.5 Ice parameters

There are two ice parameters, which have been estimated, the total ice concentration, C_{is} and the multi year ice fraction, F_{MY}. The ice concentration is, as expected, estimated to be high in the north and lower nearer to the ice edge. The standard deviation is low over the area with high ice concentration and increases at the ice edge. An example can be seen on Figure 5-7 where it also can be seen, that the standard deviation is high beneath the big cloud over the open water. In this open water area there is also estimated a small amount of sea ice.
The multi year ice fraction, F_{MY} is high were the multi year ice is expected to be, lower where the first year ice is expected to be. An example of the standard deviation of the multi year ice fraction can be seen on Figure 5-8. Here it can be seen, that the standard deviation is almost constant all over the sea ice area, except for the area at the ice edge, where the standard deviation is a little higher.
When looking at the unstable example from the 27th of October 2003, it can be seen that the ice concentration can be estimated very well (see Figure 5-34). But for the multi year ice fraction on Figure 5-35 it can be seen, that a lot of the ice, which is multi year ice, has been classified as first year ice. This phenomenon occurs especially close to the ice edge.

5.6.6 Test value

The test value reflects the ability of the inversion algorithm to model the measures brightness temperatures. The test value is the square root of the sum of squares of the differences between the modeled and the measures brightness temperatures at the 10 channels.
The test value has the largest value over the ice surface and especially at the ice edge. Furthermore the test value is also high in areas where the atmosphere contains high amounts of either water vapor or liquid water.
It should also be mentioned that even though the data sets have been masked by a land mask, it still looks like there could be a problem with some interference from land in some areas. This is especially seen in Figure 5-36 where it can be seen that the test values are very high close the coasts of England, Ireland and Iceland.

6 Conclusion

It has been demonstrated that the applied forward model of ice, ocean and the atmosphere provides a usefull framework for inversion of microwave radiometer measurements from the AMSR-E microwave radiometer.
Also it has been demonstrated how an optimal estimation technique that iterates a linear estimation model to accommodate the mild non-linearities in the forward model.

7 References

Cavalieri, Donald J. and Josefino C. Comiso. Algorithm Theoretical Basis Document (ATBD) for the AMSR-E Sea Ice Algorithm. Laboratory for Hydrospheric Processes, NASA Goddard Space Flight Center, Maryland. December 1, 2000

Comiso, Josefino C.; Donald J. Cavalieri; Claire L. Parkinson and Per Gloersen. Passive microwave algorithms for sea ice concentration: A comparison of two techniques. Remote Sens. Environ., Vol 60:357-384, 1997

Météo-France. Ocean & sea Ice SAF. North Atlantic Regional Sea Surface Temperature, Product Manual. Version 1.2. October 2002

NASDA. AMSR-E Data Users Handbook. Technical Report NCX-030021. 1st Edition. July 2003.

Pedersen, Leif Toudal. Retrieval of sea ice concentration by means of microwave radiometry. Technical Report LD81, EMI, The Technical University of Denmark, Lyngby, Denmark, February 1991.

Rodgers, C.D. Retrieval of atmospheric temperature and composition from remote measurements of thermal radiation. Reviews of Geophysics and Space Physics. Vol. 14(nr. 4): 609-624, November 1976.

Wentz, Frank J. A model function for ocean microwave brightness temperatures. Journal of Geophysical Research. Vol. 88(nr. C3): 1892-1908. 1983.

Wentz, Frank J. and Thomas Meissner. AMSR Ocean Algorithm. Algorithm Theoretical Basis Document (ATBD). Remote Sensing Systems. California, U.S. Version 2. November 2. 2002.

Wentz, Frank J. and Thomas Meissner. AMSR Ocean Algorithm. Algorithm Theoretical Basis Document (ATBD). Remote Sensing Systems. California, U.S. Version 2. November 2. 2002.